Table 1. Fluorescence activated cell sorting (FACS) analyses for the population of red fluorescent protein (RFP)- and green fluorescent protein (GFP)-positive cells in melanoma tumor

Cell lines coinoculated	Fluorescent signal used	% of total sorted cells in tumor	SD
WM1552C-RFP +	RFP	0.26	0.21
SK-Mel-2-GFP	GFP	85.9	4.72
SK-Mel-2-RFP +	RFP	3.22	1.8
SK-Mel-2-GFP	GFP	42	1.6

Formed tumors with coinoculation of indicated cell lines were isolated, dissected, and subjected to FACS analyses, n = 4.

human melanoma cell line, but not from normal melanocytes, increased migration and invasion of human mesenchymal stem cells. The CM-induced migration was inhibited by neutralization of FGF2 (Watts and Cui, 2012). Our results are consistent with these studies showing that CM of human melanoma cells increased migration of human endothelial cells via FGF2 signaling (Fig. 1). Furthermore, we have demonstrated the role of Epac1 in migration of endothelial cells via paracrine-acting FGF2 signaling, which subsequently results in increased angiogenesis (Figure 2). In addition, our results indicated the existence of FGF2-dependent cell/cell communication not only between melanoma and endothelial cells but also between melanoma and melanoma cells. This melanoma/melanoma cell communication in migration was obvious between Epac1-rich and Epac1-poor melanoma cells, but unclear between Epac1-rich and Epac1-rich melanoma cells (Figure 3C). This lacking of cell/cell communication is probably explained by saturated migration via abundant expression of Epac1 in the same cells as we have previously shown (Baljinnyam et al., 2011) and by the minimal effect of autocrine FGF2 signaling. Regarding WM1552C migration (Figure 3B), although Epac1's expression varies between the cell lines used for the study, the degree of migration did not directly reflect the degree of Epac1 expression. This was attributable, at least in part, to saturation of paracrine-acting FGF2 signaling and is supported by the data showing that FGF2 receptor expression is much higher in WM1552C cells compared with HEMA-LP (data not shown) in which the effects of CM are variable. Altogether, in terms of melanoma progression, Epac1's role in migration affects three types of cells: 1) Epac1-rich melanoma cells themselves, 2) Neighboring endothelial cells, 3) Neighboring Epac1-poor melanoma cells. Accordingly, targeting Epac1 would be an inhibitory mechanism for melanoma progression.

Perlecan is necessary for the binding of FGF2 to FGF receptor in human melanoma cells (Aviezer et al., 1997). N-sulfation of HS chains is critical for this interaction (Faham et al., 1996; Kreuger et al., 1999; Maccarana et al., 1993; Schlessinger et al., 2000). Although N-sulfation is largely regulated by NDSTs, little is known about how the expression/activity of NDSTs is regulated. We have shown that Epac1 can increase NDST-1 expression in melanoma cells (Baljinnyam et al., 2009). In addition, N-sulfation of HS was increased in the mixture of medium and cell lysate (Baljinnyam et al., 2011). In the present study, N-sulfation of secreted perlecan in the CM was reduced by Epac1 knockdown (Figure 4A). Furthermore, FGF2 binding to FGF receptor was inhibited by Epac1 knockdown (Figure 4B, C). Therefore, it is proposed that Epac1-rich melanoma cells can affect FGF2 signaling in neighboring cells via modification of N-sulfation of HS on perlecan. Meanwhile, knockdown of Epac1 reduced the amount of perlecan as demonstrated by Western blot analysis with a perlecan-specific antibody (CCN-1) (data not shown). Interestingly, expression of perlecan is regulated by the cAMP response element (CRE) as its promoter (Furuta et al., 2000). Thus, Epac1 potentially may regulate perlecan expression itself in addition to N-sulfation of HS, suggesting multiple roles of Epac1 on biosynthesis HSPG. However, further studies would be required to confirm this because another study found that Epac1 does not regulate transcription through CREB transcription factors and that the best characterized route for Epac1 to regulate transcription is through C/EBP transcription factors (Yarwood et al., 2008, JBC).

Our data showed that melanomas formed by coinoculation of Epac1-rich and Epac1-poor melanoma cells involved both melanoma populations (Figure 5D and Table 1). These data suggest that cell/cell communication within melanomas may support the survival of melanoma cells with lower malignancy potential. To confirm that Epac1 in Epac1-rich melanoma cells affect proliferation of another Epac1-poor melanoma cells, it is necessary to examine whether Epac1 knockdown decreases the number of Epac1-poor melanoma cells *in vivo*. However, inhibition of Epac1 itself affects angiogenesis as shown in our data (Figure 2), which may result in decreased proliferation of Epac1-rich (SK-Mel-2) cells themselves. Indeed, knockdown of Epac1 reduced tumor growth *in vivo* (data not shown). Therefore, knockdown of Epac1 itself may affect the local blood supply and thus survival and proliferation of Epac1-poor melanoma cells. Therefore, when Epac1 is knocked down in Epac1-rich melanoma cells, multiple factors may affect proliferation of Epac1-poor melanoma cell, suggesting difficulty of interpretation of the acquired data. Recently, specific Epac1 inhibitors have become commercially available. These inhibitors, HJC-0350 and ESI-09, indeed suppressed CM-induced migration in WM3248 cells (Figure S5), suggesting potential usage of these inhibitors for melanoma therapy, which will be addressed in our future study. Finally, HS binds to and regulates the activity of extracellular superoxide dismutase (EC-SOD), which results in increased protection against oxidative stress (Yamamoto et al., 2000). In addition, a device containing HS to deliver FGF2 enhanced FGF2's antioxidative property (Galderisi

et al., 2013). Accordingly, one could argue that Epac1 has antioxidative stress effects via the modification of HS-FGF2 signaling. Indeed, CM of SK-Mel-2 cells inhibited H_2O_2-induced apoptosis of WM1552C cells (data not shown). This antiapoptotic effect of the CM may modify the survival of WM1552C cells coinoculated with SK-Mel-2 cells *in vivo* (Figure 5), whereas rigorous examination for the protection against antioxidative stress should be performed to obtain conclusive evidence.

In summary, this study for the first time demonstrated Epac1-mediated cell/cell communication by modification of FGF2–HS interaction. Our findings may lead to a new strategy for the melanoma therapy targeting a certain population of melanoma cells, that is, Epac1-rich melanoma cells. Future research should attempt to examine the effect of Epac1-specific inhibitors on melanoma progression.

Methods

Reagents and cell lines

HEMA-LP was purchased from Invitrogen (Carlsbad, CA, USA), HUVEC was from VEC Technologies. WM1552C was from Dr. Meenhard Herlyn, Wistar Institute. C8161 cell line was provided by Dr. Mary JC Hendrix. SK-Mel-2 cells (ATCC) were maintained in MEM containing 10% FBS, 1% penicillin/streptomycin. WM1552C and C8161 cells were maintained in RPMI with 10% FBS, 1% penicillin/streptomycin. HEMA-LP and HUVEC cells were maintained in EndoGRO medium (EMD Millipore, Billerica, MA, USA) containing 5% FBS. Antibodies against Epac1, FGF2, and FGFR-1 were from Cell Signaling, anti-NDST-1 antibody was from Abnova and anti-α-tubulin antibody was purchased from Abcam (Cambridge, MA, USA).

Short hairpin RNA transduction

Short hairpin RNA (shRNA) transductions with lentivirus (Santa Cruz Biotechnology) were performed as we previously described (Baljinnyam et al., 2010). C8161 cells were incubated with 8 μg/ml of Polybrene and lentiviral particles harboring shRNA were selected with puromycin dihydrochloride for 1 week. Fresh puromycin-containing medium was replaced every 3–4 days. Established cell lines are as follows: C8161 cells with control shRNA (C8161/control), C8161 cells with Epac1 shRNA [C8161/Epac1(−)].

Migration assay

Migration assay was performed using the 24-well Boyden chambers (8 μm pores, BD Biosciences, San Jose, CA, USA) as we previously described (Baljinnyam et al., 2009). The cells were plated at a density of 1×10^6 cells/100 μl of medium in the inserts and incubated for 16 h at 37°C in the conditioned media. The insert membranes were stained using the Diff-Quick kit (Dade Behring). Pictures were taken and migrated cells were counted with Image J software using 10 randomly chosen fields.

Purification of human perlecan

About 2 L of conditioned medium for 72 h by confluent cultures of human melanoma cells was purified by DEAE–Sepharose chromatography (Whitelock et al., 1999) (100 ml bed volume, flow rate 1 ml/min) which had been equilibrated with 250 mM NaCl (20 mM Tris, 10 mM Methylenediaminetetraacetic acid, 1 mM phenylmethylsulfonyl fluoride, 1 mM benzamidine, pH 7.5). The column was washed extensively with the buffer, and bound proteins were eluted using 1 M NaCl, 20 mM Tris, 10 mM Methylenediaminetetraacetic acid. The presence of HS-bound perlecan was monitored in column fractions using antibodies to HS (10E4) in an enzyme-linked immunosorbent assay (ELISA). The protein concentration was measured using the Coomassie Plus assay (Pierce), and aliquots were stored at −70°C until used for further Western blot analyses.

Western blot analysis

Western blot analysis was performed as previously described (Iwatsubo et al., 2003, 2004). Briefly, cells were lysed and sonicated in RIPA lysis buffer. Equal amounts of protein were subjected to SDS-PAGE, were transferred to Millipore Immobilon-P membrane, and immunoblotting with respective antibodies was performed.

Tube formation assay

Human umbilical vein endothelial cells under seven passages were used in all experiments. *In vitro* angiogenesis tube formation assay was performed as we previously described with some modifications (De Lorenzo et al., 2004; Movafagh et al., 2006). HUVEC (5000/well) were seeded in 24-well plates coated with Matrigel (Biosciences Discovery), incubated in CM for 4 h at 37°C. The tube formation was quantified by counting the number of connecting branches between two discrete endothelial cells.

Immunoprecipitation

Dynabeads-Protein G for immunoprecipitation (Life Technologies, Carlsbad, CA, USA) were incubated with the primary antibodies and added to the soluble cell lysate fraction. These antibody-coated Dynabeads™, Life Technologies, Carlsbad, CA, USA bound to the target proteins were separated by the magnet and after repeated washing three times, the isolated protein complexes were subjected to SDS-PAGE and immunoblotting with respective antibodies.

FGF2-binding assay

FGF2-binding assay was performed as previously described (Reiland and Rapraeger, 1993). Briefly, HUVEC cells were plated in 24-well plate with 1.5×10^5 cells

density and incubated with and without indicated. The cells were pulsed with 50 pM ^{125}I-bFGF for 2 h at 4°C in binding buffer, washed three times with 20 mM HEPES (pH 7.4) containing 150 mM NaCl and 0.2% BSA at 4°C. Low-affinity HSPG-binding sites were detected by two collected 1-ml washes of 20 mM HEPES (pH 7.4) containing 2 M NaCl and 0.2% BSA at 4°C. High-affinity FGFR complex binding sites were detected by two collected 1-ml washes of 20 mM sodium acetate (pH 4.0) containing 2 M NaCl and 0.2% BSA at 4°C. Collected washes were counted in a Cobra 5003 counter (Packard/Perkin Elmer, Waltham, MA, USA). Control experiments were performed with unlabeled FGF2 to determine non-specific binding. Results were reported as the relative binding of experimental condition compared with untreated controls.

Generation of GFP- and RFP-labeled melanoma cells

Cells were incubated with lentiviral particles for GFP and RFP expression (Biogenova, Potomac, MD, USA) and were selected with FACS before the inoculation to obtain the cells homogenously expressing RFP or GFP. FACS cell sorting was performed by a FACS Caliburs (BD Biosciences). *In vivo* imaging of RFP- and GFP-labeled tumor cells were carried out by *in vivo* imaging system (IVIS).

Tumor growth assay

BALB/c athymic (nu/nu) mice were inoculated in the right flank with C8161 cells with or without Epac1 shRNA deletions (10^6 cells/0.1 ml culture medium) (n = 6/group). In another series of experiments, prelabeled SK-Mel-2 cells (MM, high Epac1 expression) and WM1552C cells (RGP, low Epac1 expression) were used: (a) SK-Mel-2-GFP + SK-Mel-2-RFP injected mice n = 8/group; (b) SK-Mel-2-GFP+WM-1552C-RFP cells injected mice n = 8/group; c. WM-1552C-GFP+ WM-1552C-RFP cells injected mice, n = 4/group. Tumor growth was assessed twice a week by caliper measurement of tumor diameter in the longest dimension (*L*) and at right angles to that axis (*W*) (De Lorenzo et al., 2011). Tumor volumes were estimated using the formula, $L \times W \times W \times \pi/6$. At the end of the experiment, half of each tumor was fixed by immersion in 10% phosphate-buffered formalin, dehydrated, and embedded in paraffin. Major organs were subjected to gross pathology and histology analysis to determine metastases. Studies were approved by the Animal Care and Use Committee of New Jersey Medical School.

Immunofluorescent staining

The paraffin-embedded slides of melanomas from BALB/c mice were subjected to deparaffinization in xylene, followed by treatment with a graded series of alcohols (100%, 95%, and 80% ethanol [v/v] in double-distilled H_2O) and rehydration in PBS (pH 7.5). For antigen retrieval, the sections were submerged in a boiling temperature citrate buffer (pH 6.0) for 15 m. The samples were blocked with the Image-iT FX signal enhancer (Invitrogen) to prevent non-specific staining and incubated with primary antibodies and respective secondary antibodies. Alexa Fluor 488– and 594-conjugated goat anti-rabbit and anti-mouse antibodies (Molecular Probes, Life Technologies) were used as secondary antibodies. The slides were mounted using Prolong Gold mounting media with 4′, 6-diamidino-2-phenylindole (DAPI).

For the study of RFP- and GFP-labeled cells in tumors, tissue sections from tumors were immunostained with rabbit antibody against GFP (dilution 1:100, Abcam), mouse antibody against RFP (dilution 1:200; Abcam). Negative controls without the primary antibody were performed to show specificity of the antibody.

Immunohistochemical staining

Tumor angiogenesis was evaluated by immunostaining for CD31 (dilution1:250, Santa Cruz Biotechnologies, Santa Cruz, CA, USA). Tissue sections were cut and immunostained with the primary antibody for CD31 using the standard VectaStain ABC kit (Vector Laboratories, Burlingame, CA, USA). Microvessel density was assessed by counting the number of microvessels positive for CD31 at ×400 magnification. Negative control without the primary antibody was performed at the same time.

Overexpression of Epac1

Adenoviral OE of Epac1 in melanoma cells was performed as we previously described (Baljinnyam et al., 2009).

Data analysis and statistics

Statistical comparisons among groups were performed using one-factor ANOVA with Bonferroni post hoc test. Statistical significance was set at the 0.05 level.

Acknowledgement

This study was supported by the American Heart Association (SDG 0835596D), the Foundation of UMDNJ and Melanoma Research Foundation (K. Iwatsubo).

References

Aviezer, D., Iozzo, R.V., Noonan, D.M., and Yayon, A. (1997). Suppression of autocrine and paracrine functions of basic fibroblast growth factor by stable expression of perlecan antisense cDNA. Mol. Cell. Biol. *17*, 1938–1946.

Baljinnyam, E., Iwatsubo, K., Kurotani, R., Wang, X., Ulucan, C., Iwatsubo, M., Lagunoff, D., and Ishikawa, Y. (2009). Epac increases melanoma cell migration by a heparan sulfate-related mechanism. Am. J. Physiol. Cell Physiol. *297*, C802–C813.

Baljinnyam, E., De Lorenzo, M.S., Xie, L.H., Iwatsubo, M., Chen, S., Goydos, J.S., Nowycky, M.C., and Iwatsubo, K. (2010). Exchange protein directly activated by cyclic AMP increases melanoma cell migration by a Ca2 + -dependent mechanism. Cancer Res. *70*, 5607–5617.

Baljinnyam, E., Umemura, M., De Lorenzo, M.S., Iwatsubo, M., Chen, S., Goydos, J.S., and Iwatsubo, K. (2011). Epac1 promotes melanoma metastasis via modification of heparan sulfate. Pigment Cell Melanoma Res. *24*, 680–687.

Bos, J.L. (2006). Epac proteins: multi-purpose cAMP targets. Trends Biochem. Sci. *31*, 680–686.

De Lorenzo, M.S., Farina, H.G., Alonso, D.F., and Gomez, D.E. (2004). Role of protein kinase C-dependent signaling pathways in the antiangiogenic properties of nafoxidine. Anticancer Res. *24*, 1737–1744.

De Lorenzo, M.S., Baljinnyam, E., Vatner, D.E., Abarzúa, P., Vatner, S.F., and Rabson, A.B. (2011). Caloric restriction reduces growth of mammary tumors and metastases. Carcinogenesis *32*, 1381–1387.

De Rooij, J., Zwartkruis, F.J., Verheijen, M.H., Cool, R.H., Nijman, S.M., Wittinghofer, A., and Bos, J.L. (1998). Epac is a Rap1 guanine-nucleotide-exchange factor directly activated by cyclic AMP. Nature *396*, 474–477.

Faham, S., Hileman, R.E., Fromm, J.R., Linhardt, R.J., and Rees, D.C. (1996). Heparin structure and interactions with basic fibroblast growth factor. Science *271*, 1116–1120.

Furuta, G.T., Dzus, A.L., Taylor, C.T., and Colgan, S.P. (2000). Parallel induction of epithelial surface-associated chemokine and proteoglycan by cellular hypoxia: implications for neutrophil activation. J. Leukoc. Biol. *68*, 251–259.

Galderisi, U., Peluso, G., Di Bernardo, G., Calarco, A., D'apolito, M., Petillo, O., Cipollaro, M., Fusco, F.R., and Melone, M.A. (2013). Efficient cultivation of neural stem cells with controlled delivery of FGF-2. Stem Cell Res. *10*, 85–94.

Garrido, T., Riese, H.H., Aracil, M., and Perez-Aranda, A. (1995). Endothelial cell differentiation into capillary-like structures in response to tumour cell conditioned medium: a modified chemotaxis chamber assay. Br. J. Cancer *71*, 770–775.

Gartside, M.G., Chen, H., Ibrahimi, O.A. et al. (2009). Loss-of-function fibroblast growth factor receptor-2 mutations in melanoma. Mol. Cancer Res. *7*, 41–54.

Grandoch, M., Lopez De Jesus, M., Oude Weernink, P.A., Weber, A.A., Jakobs, K.H., and Schmidt, M. (2009a). B cell receptor-induced growth arrest and apoptosis in WEHI-231 immature B lymphoma cells involve cyclic AMP and Epac proteins. Cell. Signal. *21*, 609–621.

Grandoch, M., Rose, A., Ter Braak, M., Jendrossek, V., Rubben, H., Fischer, J.W., Schmidt, M., and Weber, A.A. (2009b). Epac inhibits migration and proliferation of human prostate carcinoma cells. Br. J. Cancer *101*, 2038–2042.

Hibino, S., Shibuya, M., Hoffman, M.P., Engbring, J.A., Hossain, R., Mochizuki, M., Kudoh, S., Nomizu, M., and Kleinman, H.K. (2005). Laminin alpha5 chain metastasis- and angiogenesis-inhibiting peptide blocks fibroblast growth factor 2 activity by binding to the heparan sulfate chains of CD44. Cancer Res. *65*, 10494–10501.

Iozzo, R.V., and San Antonio, J.D. (2001). Heparan sulfate proteoglycans: heavy hitters in the angiogenesis arena. J. Clin. Invest. *108*, 349–355.

Iwatsubo, K., Toya, Y., Fujita, T., Ebina, T., Schwencke, C., Minamisawa, S., Umemura, S., and Ishikawa, Y. (2003). Ischemic preconditioning prevents ischemia-induced beta-adrenergic receptor sequestration. J. Mol. Cell. Cardiol. *35*, 923–929.

Iwatsubo, K., Minamisawa, S., Tsunematsu, T., Nakagome, M., Toya, Y., Tomlinson, J.E., Umemura, S., Scarborough, R.M., Levy, D.E., and Ishikawa, Y. (2004). Direct inhibition of type 5 adenylyl cyclase prevents myocardial apoptosis without functional deterioration. J. Biol. Chem. *279*, 40938–40945.

Knox, S., Merry, C., Stringer, S., Melrose, J., and Whitelock, J. (2002). Not all perlecans are created equal: interactions with fibroblast growth factor (FGF) 2 and FGF receptors. J. Biol. Chem. *277*, 14657–14665.

Kreuger, J., Prydz, K., Pettersson, R.F., Lindahl, U., and Salmivirta, M. (1999). Characterization of fibroblast growth factor 1 binding heparan sulfate domain. Glycobiology *9*, 723–729.

Lamalice, L., le Boeuf, F., and Huot, J. (2007). Endothelial cell migration during angiogenesis. Circ. Res. *100*, 782–794.

Lissitzky, J.C., Parriaux, D., Ristorcelli, E., Verine, A., Lombardo, D., and Verrando, P. (2009). Cyclic AMP signaling as a mediator of vasculogenic mimicry in aggressive human melanoma cells in vitro. Cancer Res. *69*, 802–809.

Little, A.S., Smith, P.D., and Cook, S.J. (2012). Mechanisms of acquired resistance to ERK1/2 pathway inhibitors. Oncogene *32*, 1207–1215.

Maccarana, M., Casu, B., and Lindahl, U. (1993). Minimal sequence in heparin/heparan sulfate required for binding of basic fibroblast growth factor. J. Biol. Chem. *268*, 23898–23905.

Maurer, G., Tarkowski, B., and Baccarini, M. (2011). Raf kinases in cancer-roles and therapeutic opportunities. Oncogene *30*, 3477–3488.

Meier, F., Nesbit, M., Hsu, M.Y. et al. (2000). Human melanoma progression in skin reconstructs: biological significance of bFGF. Am. J. Pathol. *156*, 193–200.

Meier, F., Caroli, U., Satyamoorthy, K. et al. (2003). Fibroblast growth factor-2 but not Mel-CAM and/or beta3 integrin promotes progression of melanocytes to melanoma. Exp. Dermatol. *12*, 296–306.

Montesano, R., Vassalli, J.D., Baird, A., Guillemin, R., and Orci, L. (1986). Basic fibroblast growth factor induces angiogenesis in vitro. Proc. Natl Acad. Sci. USA *83*, 7297–7301.

Moscatelli, D., Presta, M., Joseph-Silverstein, J., and Rifkin, D.B. (1986). Both normal and tumor cells produce basic fibroblast growth factor. J. Cell. Physiol. *129*, 273–276.

Movafagh, S., Hobson, J.P., Spiegel, S., Kleinman, H.K., and Zukowska, Z. (2006). Neuropeptide Y induces migration, proliferation, and tube formation of endothelial cells bimodally via Y1, Y2, and Y5 receptors. FASEB J. *20*, 1924–1926.

Nugent, M.A., and Iozzo, R.V. (2000). Fibroblast growth factor-2. Int. J. Biochem. Cell Biol. *32*, 115–120.

Ozen, M., Medrano, E.E., and Ittmann, M. (2004). Inhibition of proliferation and survival of melanoma cells by adenoviral-mediated expression of dominant negative fibroblast growth factor receptor. Melanoma Res. *14*, 13–21.

Ponta, H., Wainwright, D., and Herrlich, P. (1998). The CD44 protein family. Int. J. Biochem. Cell Biol. *30*, 299–305.

Quilliam, L.A., Rebhun, J.F., and Castro, A.F. (2002). A growing family of guanine nucleotide exchange factors is responsible for activation of Ras-family GTPases. Prog. Nucleic Acid Res. Mol. Biol. *71*, 391–444.

Reiland, J., and Rapraeger, A.C. (1993). Heparan sulfate proteoglycan and FGF receptor target basic FGF to different intracellular destinations. J. Cell Sci. *105*(Pt 4), 1085–1093.

Schlessinger, J., Plotnikov, A.N., Ibrahimi, O.A., Eliseenkova, A.V., Yeh, B.K., Yayon, A., Linhardt, R.J., and Mohammadi, M. (2000). Crystal structure of a ternary FGF-FGFR-heparin complex reveals a dual role for heparin in FGFR binding and dimerization. Mol. Cell *6*, 743–750.

Sharma, B., Handler, M., Eichstetter, I., Whitelock, J.M., Nugent, M.A., and Iozzo, R.V. (1998). Antisense targeting of perlecan blocks tumor growth and angiogenesis in vivo. J. Clin. Invest. *102*, 1599–1608.

Sola, F., Gualandris, A., Belleri, M. et al. (1997). Endothelial cells overexpressing basic fibroblast growth factor (FGF-2) induce vascular tumors in immunodeficient mice. Angiogenesis *1*, 102–116.

Taylor, W.R., Greenberg, A.H., Turley, E.A., and Wright, J.A. (1993). Cell motility, invasion, and malignancy induced by overexpression of K-FGF or bFGF. Exp. Cell Res. *204*, 295–301.

Tiwari, S., Felekkis, K., Moon, E.Y., Flies, A., Sherr, D.H., and Lerner, A. (2004). Among circulating hematopoietic cells, B-CLL uniquely expresses functional EPAC1, but EPAC1-mediated Rap1 activation does not account for PDE4 inhibitor-induced apoptosis. Blood *103*, 2661–2667.

Watts, T.L., and Cui, R. (2012). Malignant melanoma induces migration and invasion of adult mesenchymal stem cells. Laryngoscope *122*, 2769–2772.

Whitelock, J.M., Graham, L.D., Melrose, J., Murdoch, A.D., Iozzo, R.V., and Underwood, P.A. (1999). Human perlecan immunopurified from different endothelial cell sources has different adhesive properties for vascular cells. Matrix Biol. *18*, 163–178.

Yamamoto, M., Hara, H., and Adachi, T. (2000). Effects of homocysteine on the binding of extracellular-superoxide dismutase to the endothelial cell surface. FEBS Lett. *486*, 159–162.

Yarwood, S.J., Borland, G., Sands, W.A., and Palmer, T.M. (2008). Identification of CCAAT/enhancer-binding proteins as exchange protein activated by cAMP-activated transcription factors that mediate the induction of the SOCS-3 gene. J. Biol. Chem. *283*, 6843–6853.

Supporting Information

Additional Supporting Information may be found in the online version of this article:

Figure S1. Epac1 overexpression (OE) increases migration of primary melanoma cell lines. (A) Western blot of Epac1 OE in WM115 and WM3248 cells 24 h after adenoviral infection. (B) Epac1 OE increased migration of WM115 and WM3248 cells. *$P < 0.05$ versus control, $n = 4$.

Figure S2. Epac1 regulates CM-induced migration of primary melanoma cells. (A) Western blot of C8161 cells with or without Epac1shRNA (Sigma Aldrich) transduction. (B) Epac1 knockdown with Epac1 shRNA (Sigma) in C8161 cells inhibited the CM-induced migration of WM1552C cells.

Figure S3. FGF2 is involved CM-induced migration of primary melanoma. Indicated combinations of cells for the evaluation of migration and CM preparation were examined. The neutralizing FGF2 antibody reduced cell migration in all examined combinations. #, $P < 0.05$ versus CM, $n = 4$.

Figure S4. FGF2 is involved in Epac1 OE-mediated CM migration. CM of WM3248 cells with adenoviral Epac1 OE increased migration of SK-Mel-2 cells. The nFGF2 antibody inhibited the Epac1 OE-induced migration, $n = 4$.

Figure S5. Epac1 inhibitors reduce CM-induced migration. Migration of WM3248 cells was inhibited by CM of SK-Mel-24 cells were treated with indicated Epac inhibitors, $n = 4$.

Cardiovascular Research (2014) **104**, 326–336
doi:10.1093/cvr/cvu199

Decreased serum osmolality promotes ductus arteriosus constriction

Rika Aoki[1,2], Utako Yokoyama[1]*, Yasuhiro Ichikawa[1,2], Masataka Taguri[3], Shun Kumagaya[4], Ryo Ishiwata[1], Chiharu Yanai[1], Shujiro Fujita[1,2], Masanari Umemura[1], Takayuki Fujita[1], Satoshi Okumura[5], Motohiko Sato[6], Susumu Minamisawa[4,7], Toshihide Asou[8], Munetaka Masuda[9], Shiho Iwasaki[2], Shigeru Nishimaki[2], Kazuo Seki[2], Shumpei Yokota[2], and Yoshihiro Ishikawa[1]*

[1]Cardiovascular Research Institute, Yokohama City University, 3-9 Fukuura, Kanazawa-ku, Yokohama, Kanagawa 236-0004, Japan; [2]Department of Pediatrics, Yokohama City University, Yokohama, Japan; [3]Department of Biostatistics and Epidemiology, Yokohama City University, Yokohama, Japan; [4]Department of Life Science and Medical Bioscience, Waseda University Graduate School of Advanced Science and Engineering, Tokyo, Japan; [5]Department of Physiology, Tsurumi University School of Dental Medicine, Yokohama, Japan; [6]Department of Physiology, Aichi Medical University, Nagakute, Japan; [7]Department of Cell Physiology, Jikei University School of Medicine, Tokyo, Japan; [8]Department of Cardiovascular Surgery, Kanagawa Children's Medical Center, Yokohama, Japan; and [9]Department of Surgery, Yokohama City University, Yokohama, Japan

Received 14 February 2014; revised 8 August 2014; accepted 15 August 2014; online publish-ahead-of-print 4 September 2014

Time for primary review: 29 days

Aims At birth, dynamic changes occur in serum components and haemodynamics, such as closure of the ductus arteriosus (DA). A previous study demonstrated that, in full-term human neonates, serum osmolality decreased transiently after birth, but recovered over the next few days. However, the significance of this transient decrease in osmolality has never been addressed. The objective of the present study was to examine the role of changes in serum osmolality after birth in DA closure.

Methods and results We found that rats exhibited a similar transient hypoosmolality after birth. Hypotonic stimulation induced constriction of DA rings and increased Ca^{2+} transient in DA smooth muscle cells, but not in the aorta. The hypoosmotic sensor transient receptor potential melastatin 3 (TRPM3) was highly expressed in the rat DA, and TRPM3 silencing abolished the Ca^{2+} response to hypoosmolality. Pregnenolone sulfate stimulation of TRPM3 induced rat DA constriction *ex vivo* and *in vivo*. Furthermore, *hyper*tonic fluid injection impaired rat DA closure. In humans, neonatal serum hypoosmolality was observed in relatively mature preterm infants ($\geq$28 weeks). In extremely preterm infants ($<$28 weeks), however, this hypoosmolality was absent. Instead, a rapid increase in osmolality occurred thereafter. Such an increase was greater, in particular, among patent DA (PDA) patients.

Conclusions A transient decrease in serum osmolality may promote DA closure during the first few days of life. Adjusting serum osmolality to proper levels might help to prevent the onset of PDA, improving the therapeutic outcome in extremely preterm infants.

Keywords Patent ductus arteriosus • Paediatrics • Biology • Developmental • Osmolality • TRP channel

1. Introduction

At birth, the separation of the foetus from its maternal environment constitutes a dramatic change for the infant, as it moves from an aquatic to an atmospheric environment. Infants must start breathing with their lungs immediately and are suddenly exposed to conditions of high oxygen tension. It appears that certain specific physiological processes take place in reaction to these environmental stresses to modify the cardiovascular system and thus rapidly adapt the infant to the postnatal environment. A prime example is the closure of the ductus arteriosus (DA), which is an arterial shunt vessel connecting the pulmonary artery with the aorta.[1]

In the foetus, the DA diverts ventricular output away from the high-resistance pulmonary vascular bed into systemic circulation. Although its patency is essential for foetal circulation, once pulmonary circulation is established, the DA must be closed. Persistent patent DA (PDA) after

* Corresponding author. Tel: +81 45 787 2575; fax: +81 45 787 1470, Email: utako@yokohama-cu.ac.jp, yishikaw@med.yokohama-cu.ac.jp

birth often causes serious problems in very premature infants, depending on the degree of left-to-right shunting. It has been reported that more than 50% of infants with birth weights <1000 g receive pharmacological therapy consisting of cyclooxygenase (COX) inhibitors or surgical ligation of the DA to prevent respiratory distress, heart failure, intraventricular haemorrhage/brain injury, bronchopulmonary dysplasia, or necrotizing enterocolitis.[2–5] Because the current pharmacological and surgical therapies for treating PDA are not always ideal,[6–8] it is highly desirable to find a relatively simple and non-invasive strategy that would prevent PDA from occurring.

It is well known that increasing oxygen tension in the arteries promotes DA constriction by inhibiting voltage-gated potassium channels[9,10] and activating voltage-gated calcium channels.[11–13] Simultaneous withdrawal of placental prostaglandin E_2 (PGE_2) and promotion of PGE_2 catabolism in the lungs also contribute to DA closure.[14–16] Thus, changes in serum composition, as induced by the initiation of respiration, significantly affect closure of the DA. The onset of respiration is also known to facilitate alveolar fluid absorption in the lungs,[17–19] which may also lead to changes in serum osmolality. In this regard, it was reported convincingly by Feldman and Drummond[20] that full-term infants exhibit low serum osmolality for the very first few days of life, and that their level of serum osmolality reaches adult levels by the fifth day of life. The significance of this transient decrease in serum osmolality has been largely overlooked in infants, including premature infants, who frequently suffer from PDA.

Under physiological conditions, body fluid osmolality is tightly regulated to near 300 mOsm/kg through the intake or excretion of water and salt.[21] This homeostatic osmoregulation is vital, and hypotonicity is sensed, at least in part, by transient receptor potential (TRP) channels, such as TRP vanilloid 4 (TRPV4)[22] or TRP melastatin 3 (TRPM3),[23,24] which act as Ca^{2+} channels. Because changes in intracellular Ca^{2+} ($[Ca^{2+}]_i$) are related to DA constriction,[11–13] we hypothesized that the transient decrease in serum osmolality may contribute to DA closure, potentially via TRP channels.

In this study, we demonstrated a similar transient decrease in serum osmolality at birth in rat neonates, as previously reported in human neonates by Feldman *et al.*[20] Furthermore, we found that hypoosmolality contributed to the constriction of the DA through the activation of TRPM3 in rats. We also demonstrated that this transient decrease is observed in relatively mature human preterm infants, but is absent in extremely preterm infants. Extremely preterm infants with PDA, in particular, exhibited early elevation of serum osmolality. We thus suggest that serum osmolality plays an important role in regulating DA constriction, and that adjusting serum osmolality to proper levels might contribute to DA closure among extremely preterm infants.

2. Methods

Detailed information in the Methods section used in this study can be found in Supplementary Material online.

2.1 Reagents

Anti-TRPM3 antibody was purchased from Novus Biologicals (Littleton, CO, USA). Pregnenolone sulfate, a TRPM3 channel stimulator, was purchased from Sigma-Aldrich (St Louis, MO, USA). Isosakuranetin, a TRPM3 channel inhibitor, was purchased from Extrasynthese (Genay, France). Nicardipine hydrochloride was purchased from Wako (Osaka, Japan). Indomethacin was purchased from Calbiochem (San Diego, CA, USA). KB-R7943, an NCX inhibitor, was purchased from Calbiochem.

2.2 Animal studies

Wistar rat foetuses and neonates were obtained from timed-pregnant mothers purchased from Japan SLC, Inc. (Shizuoka, Japan). The experiments were approved by the Yokohama City University Institutional Animal Care and Use Committee in accordance with the Guide for the Care and Use of Laboratory Animals (reference number: F-A-13-006).

2.3 Human studies

Protocols for using blood samples and human tissues were approved by the Research Ethics Committee in Yokohama City University Hospital and Kanagawa Children's Medical Center (reference numbers: B100107034 and D13021010) and conformed to the principles outlined in the Declaration of Helsinki.

2.4 Primary culture of rat DA and aorta smooth muscle cells

Immediately after euthanasia of the mother rat using 200 mg/kg of pentobarbital, the foetuses were obtained by the caesarean section. After decapitation of the foetuses, vascular smooth muscle cells (SMCs) in primary culture were obtained from the DAs (DASMCs) and the aortas (ASMCs) of rat foetuses at the 21st day of gestation (e21) as previously described.[12,25] A single line of SMCs were obtained from about 10 rats. More than four lines of SMCs were used for each experiment. The subconfluent cells of three to six passages were used in the experiments.

2.5 Serum osmolality measurement

Serum osmolalities during the perinatal period in rats and humans were analysed by a freezing-point depression osmometer (model 210, Fiske Associates, Norwood, MA, USA). Blood samples from rat foetuses at e21 and infant rats at Day 0 (1 or 2 h after birth), Day 1, Day 2, and Day 7 were obtained by heart puncture after rats were anaesthetized with isoflurane. To obtain e21 rat foetuses and Day 0 rat infants by the caesarean section, the maternal rats at e21 were euthanized with 200 mg/kg of pentobarbital. The rat neonates over Day 1 were normally delivered and raised by their mothers until the day of measurement.

Human infants were enrolled in the study after parental written informed consent was obtained. Sixty-two total preterm infants who were admitted to the neonatal intensive care unit (NICU) of Yokohama City University Hospital at ≥24 and <36 weeks of gestation were recruited prospectively between October 2010 and March 2013. Exclusion criteria were major congenital anomalies, congenital heart diseases, and death in the first week of life. The patients were divided into two groups: those with ≥28 weeks of gestation and those with <28 weeks of gestation. The <28-week group was subdivided into PDA and non-PDA groups. In the ≥28-week group, there was only one patient with PDA. In this study, PDA was defined as the necessity of indomethacin therapy within the first week of life. Indomethacin is not prophylactically administrated at this institution. The patients were followed up until 7 days after birth.

Clinical backgrounds were recorded and are summarized in *Table 1*. Extremely preterm infants with PDA were treated with intravenous injection of indomethacin between Day 1 and Day 5 (2.1 ± 1.4 days). None of the infants received indomethacin before the osmolality measurement of Day 1, and 11 of 15 cases (73.3%) received this therapy on Day 1 or Day 2. Respiratory distress syndrome (RDS) was defined as any situation in which surfactant was administered for therapy. Cord blood (CB) samples were obtained at the time of delivery and samples from neonates were collected on admission to the NICU (1 h after birth) and on Days 1 (9–29 h after birth) and 2 (33–53 h after birth) after birth. All the samples used to test serum osmolality were centrifuged at 845 *g* for 5 min and the serum samples were kept frozen at −30°C until analysis.

Table 1 Characteristics of the preterm infant groups

Variables	A	B	C	*P*-value			
	28–35 weeks ($n = 35$)	24–27 weeks without PDA ($n = 12$)	24–27 weeks with PDA ($n = 15$)	A vs. B vs. C	A vs. B	A vs. C	B vs. C
Gestational age (weeks)	32.56 ± 2.20	26.6 ± 1.06	26.1 ± 0.95	<0.001‡	<0.001‡	<0.001‡	0.365
Birth weight (g)	1617.1 ± 512.5	823.0 ± 244.7	782.9 ± 201.6	<0.001‡	<0.001‡	<0.001‡	0.733
Male, *n* (%)	20 (57%)	5 (42%)	9 (60%)	0.584			
RDS, *n* (%)	8 (23%)	8 (67%)	10 (67%)	0.003†	0.012*	0.009†	1.000
Maximum FiO_2 in 12 h	0.32 ± 0.15	0.53 ± 0.25	0.48 ± 0.21	<0.001‡	0.001†	0.003†	0.641
SFD, *n* (%)	10 (29%)	5 (42%)	3 (20%)	0.430			
Apgar score at 1 min	6.9 ± 2.1	5.4 ± 2.4	5.0 ± 1.5	0.002†	0.027*	<0.001‡	0.603
Apgar score at 5 min	8.3 ± 1.5	7.3 ± 1.7	7.4 ± 1.6	0.019*	0.094	0.016*	0.980
Infection, *n* (%)	1 (3%)	2 (17%)	2 (13%)	0.244			
Antenatal steroids, n (%)	15 (43%)	11 (92%)	14 (93%)	<0.001‡	0.006†	0.001†	1.000
Furosemide, *n* (%)	0 (0%)	0 (0%)	2 (14%)	0.172			

RDS: respiratory distress syndrome; SFD: small for date.
*$P < 0.05$.
†$P < 0.01$
‡$P < 0.001$ statistically significant.

2.6 Osmolyte measurement

Serum Na^+, K^+, glucose, and urea nitrogen (BUN) were measured using an i-STAT blood analysis system (Abbott Laboratories, Princeton, NJ, USA).

2.7 RNA isolation and quantitative reverse transcription–polymerase chain reaction

Pooled tissues of the DA and the aorta were obtained from rat e19 foetuses ($n > 40$), e21 foetuses ($n > 40$), and neonates on the day of birth (Day 0, $n > 40$). Before tissue collection, rat foetuses were decapitated and neonates were anaesthetized with isoflurane. After the total RNA was isolated, reverse transcription–polymerase chain reaction was performed using a PrimeScript RT reagent kit (TaKaRa Bio, Tokyo, Japan) and SYBR Green (Applied Biosystems, Foster City, CA, USA). The sequences of the primers for the TRP isoforms are described in Supplementary material online, *Table S1*.

2.8 Immunohistological staining

DA tissues from rat Day 0 neonates and DA tissues from human neonates obtained during cardiac surgery were stained for TRPM3.

2.9 Isometric tension of the DA vascular rings

Isometric tension of the vascular rings of the DA ($n = 8$) and the aorta ($n = 7$) from rat e21 foetuses was measured as previously described.[13,26] The DA and aortic rings were independently isolated after decapitation from eight and seven rats, respectively. After a vasoconstriction plateau had been attained, osmolality of the bath fluid was reduced step by step from 300 to 220 mOsm/kg. Vasoconstriction at 250 mOsm/kg was also observed over 30 min in other DA rings ($n = 5$). Vasoconstriction induced by pregnenolone sulfate, a TRPM3 channel stimulator, was measured in the DA rings. The vasoconstrictions induced by hypoosmolality (250 mOsm/kg, $n = 4$) or pregnenolone sulfate (200 μmol/L, $n = 4$) were measured under pre-treatment of the TRPM3 inhibitor isosakuranetin[27,28] (25 μmol/L). Hyperosmotic relaxation of the DA ring was evaluated in indomethacin-induced DA constriction. The degree of vascular constriction was expressed as a percentage of the constriction induced by 120 mmol/L of KCl.

2.10 Intracellular Ca^{2+} concentration ($[Ca^{2+}]_i$) in SMCs

DASMCs or ASMCs obtained from more than 40 foetuses were placed in 96-well microplates at 1×10^4 cells/well. After 2 days of incubation, SMCs were loaded with 5 μmol/L of fura-2/AM (Dojindo, Kumamoto, Japan) in Tyrode solution for 20 min at 37°C. Hypotonic stimulation was induced by adding Tyrode solution containing no NaCl into each well, which induced an osmolality reduction by changing the NaCl concentration. The data were obtained from four independent experiments assayed in triplicate using four lines of SMCs.

2.11 RNA interference

Small interfering RNA (siRNA) of TRPM3 and control siRNA were purchased from Thermo Fisher Scientific (Waltham, MA, USA). According to the manufacturer's instructions, cultured DASMCs were transfected with siRNA targeted for TRPM3 using Lipofectamine RNAiMAX (Invitrogen).[26] We examined the mRNA expressions of all TRPM isoforms, and found that TRPM3, TRPM4, and TRPM7 were abundantly expressed in the rat DA, and expressions of the other isoforms were faint (data not shown). TRPC1 has been reported to contribute to DA contraction,[29] and TRPV4 is known to be activated with hypoosmolality.[22] Therefore, we examined the off-target effect of TRPM3-targeted siRNA on the abovementioned TRP channels. Efficacy of TRPM3 silencing and off-target effects on other TRP isoforms were analysed using the data from four lines of SMCs.

2.12 Rapid whole-body freezing method

A whole-body freezing method was used to examine the *in situ* morphologies and inner diameters of foetal and neonatal rat DA specimens as previously described.[26] Briefly, after the maternal rats were anaesthetized with isoflurane, *in utero* foetuses at e21 were injected intraperitoneally with pregnenolone sulfate (100 mg/kg of body weight) or indomethacin (2 mg/kg of body weight). The adequacy of anaesthesia was monitored by assessment of skeletal muscle tone, respiration rate, and response to tail pinch. After 1 h, they were delivered by the caesarean section and immediately frozen in liquid nitrogen before breathing. Other rat neonates delivered at e21 by the caesarean section were injected intraperitoneally with NaCl solution (0.15–1.5 mol/L) at birth to modulate serum osmolality. After 30 min, rat neonates were anaesthetized with isoflurane and frozen in liquid nitrogen. After

caesarean section, the maternal rats were euthanized by 200 mg/kg of pentobarbital. The frozen specimens were sectioned under a microscope, and the inner diameters of the DA, the pulmonary artery (PA), and the aorta were measured. DA/PA ratios were used to evaluate *in vivo* DA constriction.

2.13 Statistical analysis

All values are shown as the mean ± SEM of more than three independent experiments, except the characteristics of the patients, which are expressed as the mean ± SD. Detailed statistical analysis is shown in Supplementary material online. A value of $P < 0.05$ was considered significant.

3. Results

3.1 Hypotonic stimulation contracted the rat DA

As reported previously in human neonates,[20] we found that serum osmolality was also transiently decreased in rat neonates. In full-term rat neonates, it was decreased by >20 mOsm/kg within 1 h after birth (*Figure 1A*) and reached normal adult levels over the next several days. We then examined the potential role of this hypoosmolality in the

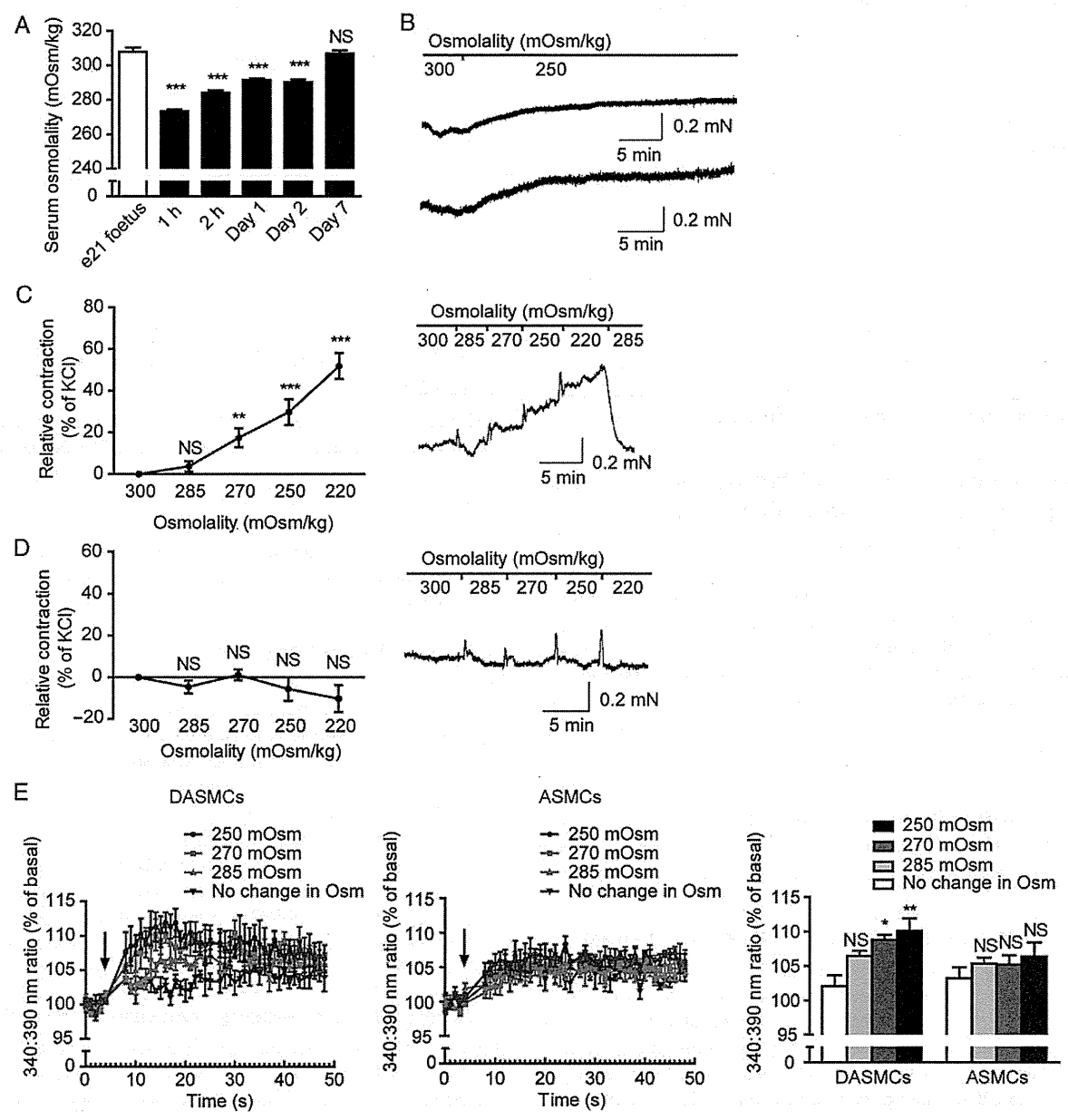

Figure 1 Effect of hypotonic stimulation on DA contraction and $[Ca^{2+}]_i$ transients in rats. (*A*) The time course of serum osmolalities in full-term rat neonates shows the transient decrease in serum osmolality after birth. $n = 4–8$, $^{***}P < 0.001$ vs. e21 foetus. NS: not significant. (*B*) Representative myograph traces of tension in the rat DA rings stimulated with hypoosmolality (250 mOsm/kg). (*C* and *D*) Effects of hypotonic stimulation on the DA (*C*) and aorta (*D*), with representative myographs. Contraction of vascular rings from full-term e21 rat foetus was measured using a wire myograph. $n = 7$-8, $^{**}P < 0.01$; $^{***}P < 0.001$ vs. 300 mOsm/kg. NS: not significant. (*E*) $[Ca^{2+}]_i$ transients were measured using fura-2 in DASMCs (left) and ASMCs (middle). Cells were incubated at 300 mOsm/kg, followed by hypotonic stimulation as indicated by arrows. Quantification at 15 s after hypotonic stimulation shows that $[Ca^{2+}]_i$ transients were specific to the DA (right). $n = 4$, $^{*}P < 0.05$; $^{**}P < 0.01$ vs. no change in osmolality. NS: not significant; mOsm: mOsm/kg.

DA, using isolated rat DA rings and a wire myograph. Hypoosmolality was generated by modulating the Na^+ concentration, a major component in serum osmolality. We found that rat DA rings contracted at 250 mOsm hypotonic stimulation (*Figure 1B*), and that the contraction was in a hypoosmolality-dependent manner (down to 220 mOsm) (*Figure 1C*, left). This contraction was reversible when osmolality was restored to 285 mOsm (*Figure 1C*, right). In contrast, hypoosmolality-induced contraction was absent in the aortic tissue rings (*Figure 1D*). It is unlikely that the Na/Ca exchanger (NCX) plays a role in this hypoosmolality-induced regulation, since inhibition of NCX by KB-R7943 did not alter hypoosmolality-induced DA contraction (see Supplementary material online, *Figure S1*).

To explore the molecular mechanisms for this DA contraction, we measured $[Ca^{2+}]_i$, which most likely regulates DA constriction, using fura-2 in DASMCs and ASMCs. When these tissues were exposed to a hypotonic solution, $[Ca^{2+}]_i$ was increased in an osmolality-dependent manner in DASMCs (*Figure 1E*, left), but not in ASMCs (*Figure 1E*, middle). Thus, osmotic sensor(s) appear to play a role only in DASMCs (*Figure 1E*, right). These data suggest that serum osmolality is physiologically decreased after birth, and that the hypoosmolality induces a postnatal contraction in the DA by regulating $[Ca^{2+}]_i$.

3.2 Hypoosmotic sensing is mediated by TRPM3 in rat DASMCs

TRP channels are known to act as osmotic sensor molecules. In particular, it has been reported that TRPV4 and TRPM3 are activated by hypoosmolality.[22–24] We found that mRNA expression of TRPM3 was greater in the rat DA than in the aorta during development, i.e. preterm (e19) and full-term (e21) foetuses as well as normal newborn neonates (d0) (*Figure 2A*). In contrast, TRPV4 mRNA expression was similar in both the DA and the aorta (*Figure 2B*). The protein expression of TRPM3 was most abundant in the medial layer of the rat DA (*Figure 2C*) and in the human DA (see Supplementary material online, *Figure S2*). We also examined the role of TRPM3 in hypoosmolality-induced elevation of $[Ca^{2+}]_i$. Hypotonic stimulation induced changes in $[Ca^{2+}]_i$ (*Figure 1E*), but such changes disappeared when TRPM3 was silenced by siRNA (*Figure 3A–C*). The TRPM3-targeted siRNA did not decrease some other TRP channels, i.e. TRPC1, TRPV4, TRPM4, and TRPM7 (see Supplementary material online, *Figure S3*). In addition, when DASMCs were preincubated with the TRPM3 inhibitor isosakuranetin, hypotonic stimulation-induced $[Ca^{2+}]_i$ elevation was attenuated (*Figure 3D*). The voltage-gated Ca^{2+} channel is activated by TRP channel-mediated Ca^{2+} influx. We therefore then examined the involvement of a voltage-gated Ca^{2+} channel, and found that the voltage-gated Ca^{2+} channel blocker nicardipine did not suppress the hypoosmolality-induced $[Ca^{2+}]_i$ elevation (*Figure 3E*). Thus, expression of TRPM3 may be responsible for osmolality-induced contraction of the DA.

3.3 Pharmacological stimulation of TRPM3 caused contraction of the rat DA

Similarly, pregnenolone sulfate, a TRPM3 stimulator,[30] increased the rat DA ring tension *in vitro* in a dose-dependent manner (*Figure 4A*). We also injected pregnenolone sulfate into rat foetuses intraperitoneally *in utero* and found that DA closure was moderately but significantly facilitated (*Figure 4B*), although this contraction was less than that caused by indomethacin, a COX inhibitor and thus a potent DA contracting drug. Furthermore, inhibition of TRPM3 using isosakuranetin attenuated the DA ring contraction induced by hypoosmotic stimulation (*Figure 4C*) or pregnenolone sulfate stimulation (*Figure 4D*). Taken together, these findings suggest that changes in osmolality regulate Ca^{2+} transients in the DA via TRPM3, resulting in DA contraction, at least, in rats.

3.4 Serum hyperosmolality suppressed DA closure

Based on the above findings, we assumed that serum *hyper*osmolality would, in contrast, inhibit DA closure. We injected the same volume of various concentrations of NaCl into rat neonates to increase their serum osmolality. Injecting 0.15 mol/L of NaCl resulted in 285.8 mOsm/kg of serum osmolality and did not alter DA closure (*Figure 5A–B*). In contrast, injecting higher concentrations of NaCl (0.6–1.5 mol/L) increased serum osmolality and inhibited DA closure in a serum osmolality-dependent manner (*Figure 5A–B*). We then examined the involvement of the inhibition of TRPM3 in *hyper*osmolality-induced DA dilation. We found that *hyper*osmolality dilated indomethacin-induced DA ring contraction; however, this was not affected by the inhibition of TRPM3 through the use of isosakuranetin (*Figure 5C*). These findings suggest that an acute increase in serum osmolality could inhibit DA closure, although this does not appear to involve TRPM3.

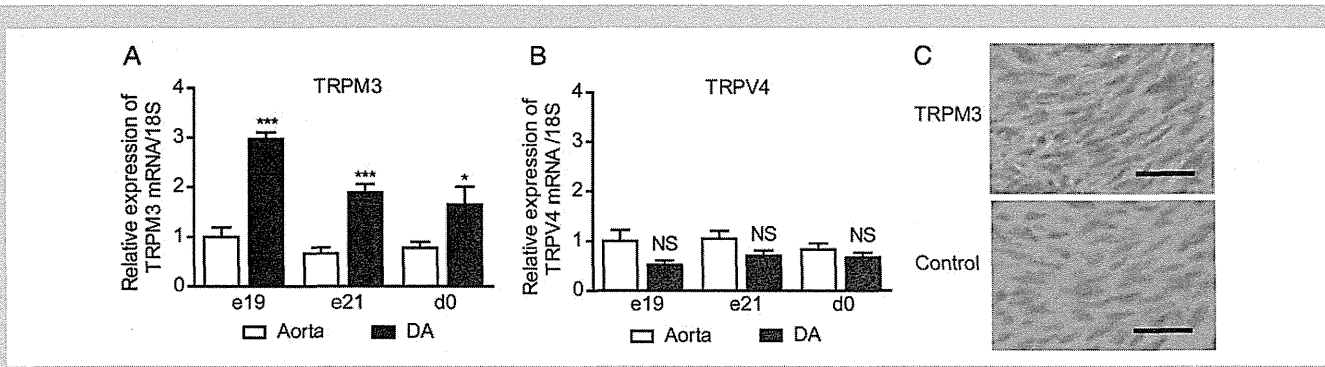

Figure 2 Expression of TRPM3 in the rat DA. (*A* and *B*) Developmental changes in the expression of TRPM3 and TRPV4 mRNA in the rat DA and aorta. $n = 4–5$, $^*P < 0.05$; $^{***}P < 0.001$ vs. the aorta. NS: not significant. (*C*) Brown colour indicates TRPM3 protein expressed in the medial layer of rat DA. Negative control (lower panel) was obtained by omission of a primary antibody. Scale bars: 20 μm.

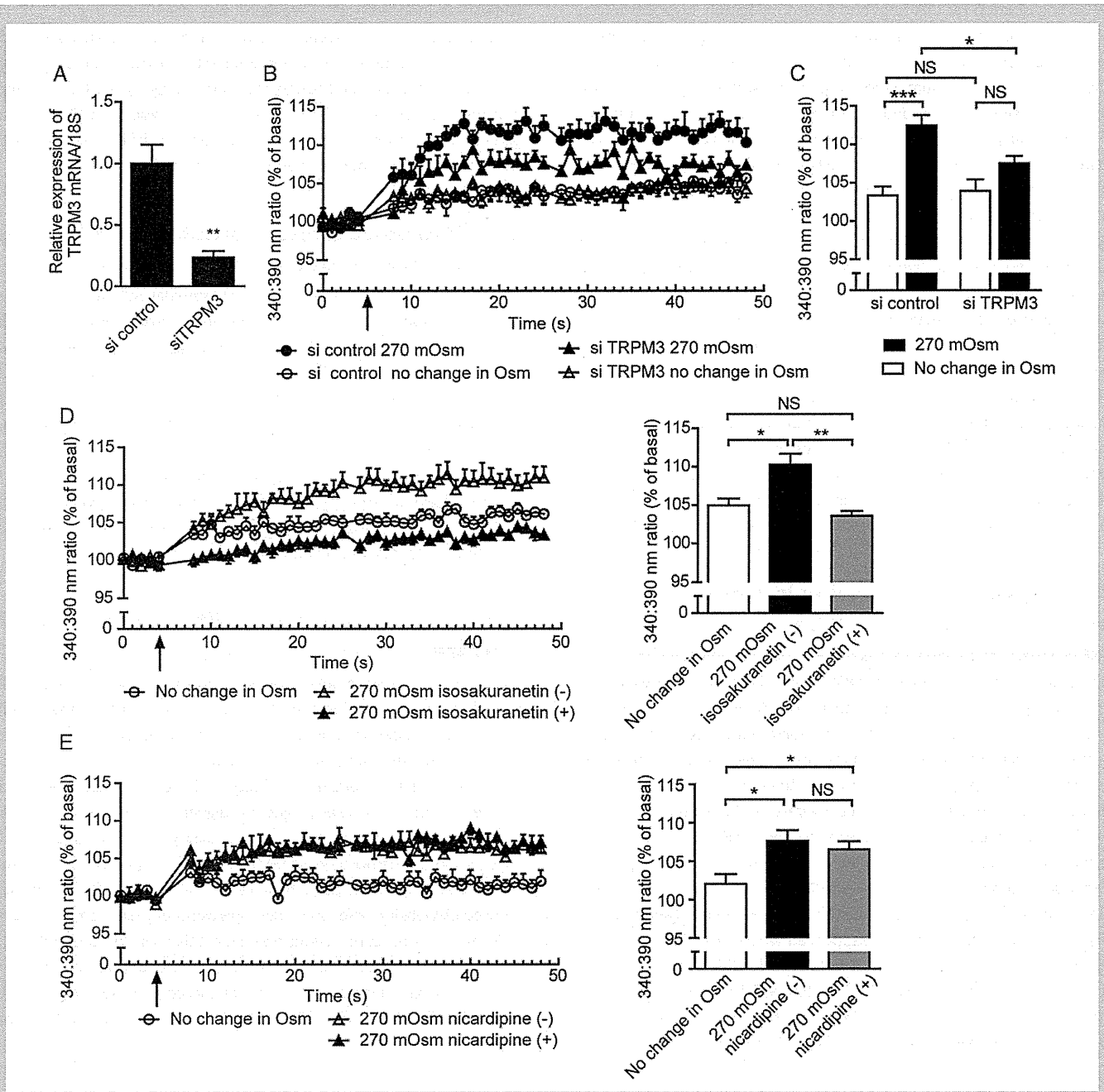

Figure 3 Hypoosmolality-induced elevation of $[Ca^{2+}]_i$ in DASMCs. (*A*) TRPM3 mRNA expression was decreased by TRPM3-targeted siRNA (si TRPM3). $n = 6$, $^{**}P < 0.01$ vs. control siRNA (si control). (*B*) $[Ca^{2+}]_i$ transients were measured using fura-2 in DASMCs treated with TRPM3-targeted siRNA or control siRNA. Cells were incubated at 300 mOsm/kg, followed by hypotonic stimulation (270 mOsm/kg) as indicated by the arrow. $n = 4$. (*C*) At 15 s after hypotonic stimulation, it can be seen that si TRPM3 eliminated the hypotonically induced $[Ca^{2+}]_i$ transients. $n = 4$, $^{*}P < 0.05$; $^{***}P < 0.001$; NS: not significant. (*D*) Preincubation of the TRPM3 inhibitor isosakuranetin (25 μmol/L) eliminated the hyposmotically induced $[Ca^{2+}]_i$ transients. $n = 5$, $^{*}P < 0.05$; $^{**}P < 0.01$; NS: not significant. (*E*) Preincubation of nicardipin (10 μmol/L) did not alter the hypotonically induced $[Ca^{2+}]_i$ transients. $n = 5$, $^{*}P < 0.05$; NS: not significant. mOsm: mOsm/kg.

3.5 Postnatal changes of serum osmolality in human preterm infants

Our data in rats demonstrated that *hypo*osmolality promoted DA constriction and that *hyper*osmolality inhibited DA closure. Since PDA develops in preterm infants in humans, we examined the relationship between PDA and serum osmolality. We measured serum osmolality of preterm infants in three groups: (i) infants delivered at 28–35 weeks of gestation (28–35-WG, moderate-preterm, and late-preterm infants, $n = 35$), (ii) infants delivered at 24–27 weeks of gestation with PDA (24–27-WG PDA+, extremely preterm infants, $n = 15$), and (iii) infants born at 24–27 of gestation without PDA (24–27-WG PDA−, extremely preterm infants, $n = 12$) (*Table 1*). Serum osmolality was determined with CB (equivalent to foetal blood at the time of birth), infant blood at Day 0 (1 h after birth), Day 1, and Day 2.

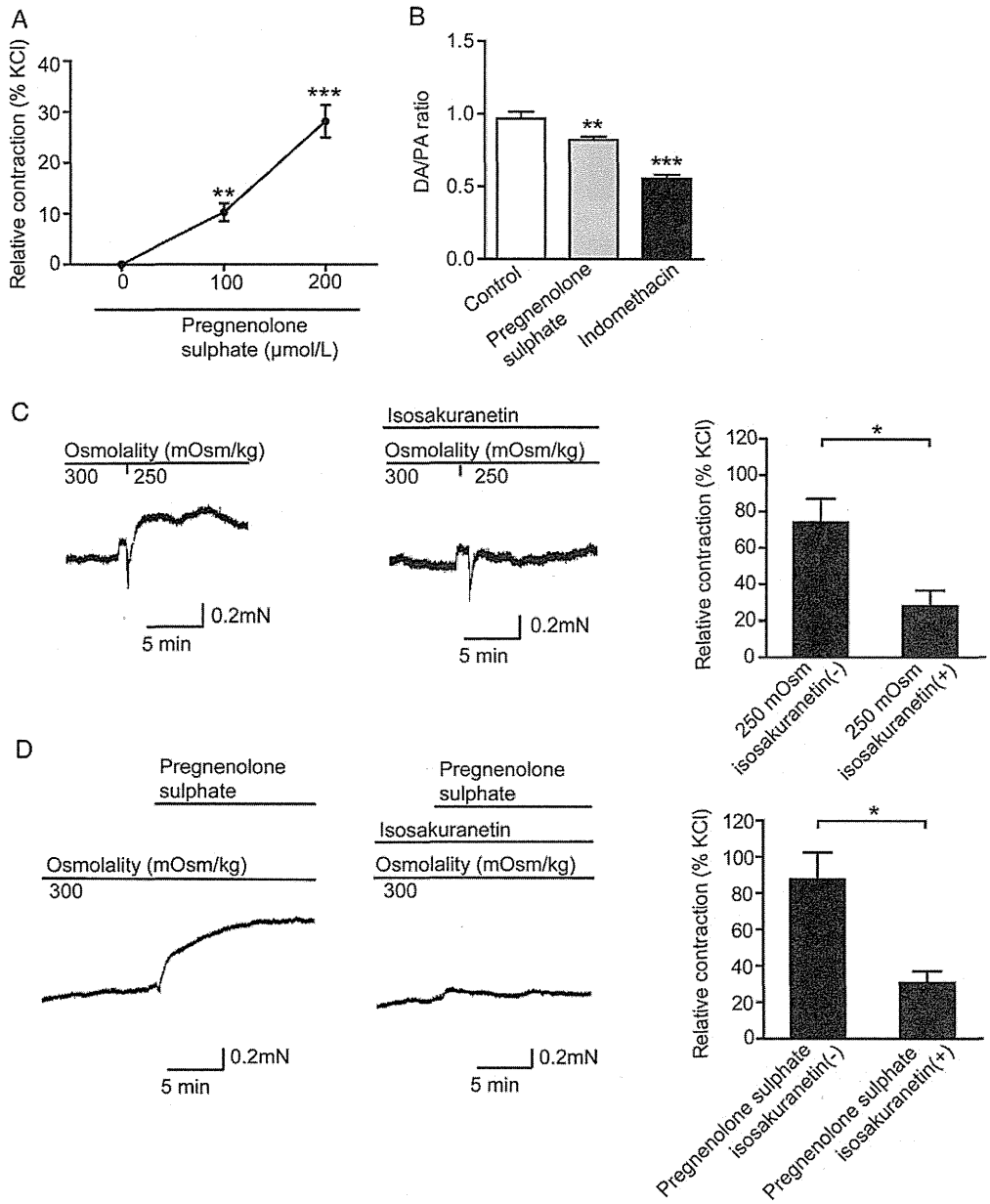

Figure 4 Effect of pregnenolone sulfate on rat DA contraction. (*A*) The TRPM3 activator pregnenolone sulfate constricted the rat e21 DA. Vascular tension was measured using a wire myograph. $n = 6$, $^{**}P < 0.01$; $^{***}P < 0.001$ vs. control. (*B*) Intraperitoneal administration of pregnenolone sulfate (100 mg/kg body weight) or indomethacin (2 mg/kg body weight) constricted e21 foetal DA *in vivo*. Diameters of the DA and the main trunk of the pulmonary artery were measured by the whole-body freezing method. $n = 4$–9, $^{**}P < 0.01$; $^{***}P < 0.001$ vs. control. (*C* and *D*) Isosakuranetin (25 μmol/L) attenuated the hypoosmotically- and pregnenolone sulfate (200 μmol/L)-induced DA contraction, respectively. Vascular tension was measured using a wire myograph. $n = 4$–6, $^{*}P < 0.05$ (*C*), $n = 4$–5, $^{*}P < 0.05$ (*D*). mOsm: mOsm/kg.

First we analysed all the groups of infants and found that serum osmolality significantly decreased at birth and gradually recovered to levels of CB (*Figure 6A*). In accordance with these data, in 28–35-WG infants, serum osmolality was decreased significantly after birth (CB vs. Day 0; 284.2 ± 1.6 vs. 275.1 ± 1.5, $P < 0.001$) and recovered to levels of CB at Day 2 (284.2 ± 1.6 vs. 284.9 ± 1.9, NS; *Figure 6B*). This pattern was consistent with data on full-term human[20] and rat neonates. In both 24–27-WG groups, however, serum osmolality was scarcely decreased at Day 0, but was significantly elevated thereafter (Days 1 and 2; *Figure 6B*). Importantly, this elevation was significantly greater in the 24–27-WG PDA+ group than in the 24–27-WG PDA− group or the 28–35-WG group (*Figure 6C*). Such dynamic differences were observed only between Day 0 and Day 1 among the three groups (*Figure 6D–E*). Thus, relatively mature infants (28–35-WG) exhibited a transient decrease and gradual recovery in serum osmolality after birth. This decrease did not occur in immature infants (24–27-WG) and rather steeply increased between Day 0 and Day 1, and this increase was much greater in infants with PDA.

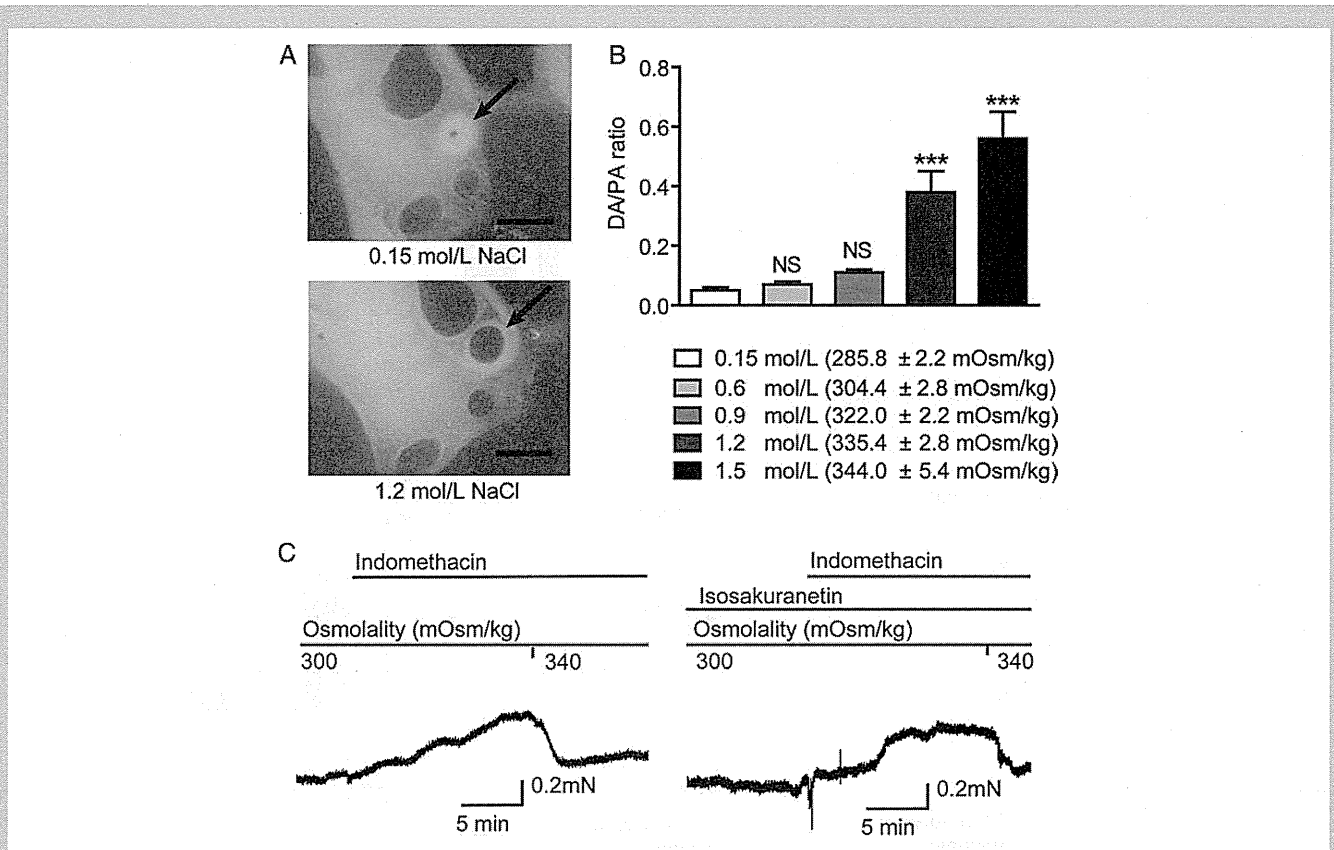

Figure 5 Inhibition of DA closure by hypertonic stimulation in rat neonates. (*A*) Representative images of rat DAs (arrows) 30 min after hypertonic stimulation with 100 μL of 0.15 mol/L NaCl (normal saline) or 1.2 mol/L NaCl. Hypertonic stimulation was induced by an intraperitoneal injection of NaCl at birth, and its effect was measured 30 min after birth using the whole-body freezing method. Scale bars: 500 μm. (*B*) Hypertonic stimulation inhibited the DA closure *in vivo*. $n = 4–8$, $^{***}P < 0.001$ vs. 0.15 mol/L. NS: not significant. (*C*) Hypertonic stimulation dilated the rat DA rings under stimulation of indomethacin ($1 \times 10^{-5.5}$ mol/L), which was not modulated by isosakuranetin (25 μmol/L). Vascular tension was measured using a wire myograph and representative myograph traces of tension are shown.

3.6 Changes in osmolality and osmolytes

Serum osmolality is regulated mainly by Na^+, K^+, BUN, and glucose. This regulation can be approximately expressed by the following formula: serum osmolality = $2(Na^+ + K^+)$ + glucose/18 + BUN/2.8. To understand which component is the cause of the changes in serum osmolality in preterm infants, these osmolytes were measured in CB and blood samples after birth. Patients' profiles for osmolytes analysis are shown in Supplementary material online, *Table S2*. Changes in serum Na^+ concentration were significantly correlated with those in serum osmolality (*Figure 7A*). No correlation between serum osmolality and K^+, BUN, or glucose was observed (*Figure 7B–D*).

4. Discussion

We have demonstrated that serum osmolality decreases after birth and gradually increases over the next few days, even in moderate- and late-preterm human infants. These findings are similar to those reported in a study performed in the late 1960s, in which it was found that serum osmolality of normal full-term infants was depressed after birth and rose to normal adult levels by Day 5.[20] We have further demonstrated in this study that extremely preterm infants showed no such early decrease, but exhibited a rapid increase in serum osmolality. This was particularly so among those infants with PDA. Using rat DAs, we then provided evidence supporting the hypothesis that serum hypoosmolality promotes DA closure, and that the mechanism most likely involves the hypoosmolality sensor TRPM3. Accordingly, although serum osmolality *per se* has been largely ignored in the past few decades, it may play an important role in regulating DA closure.

Since hypoosmolality raises $[Ca^{2+}]_i$ in rat DASMCs and increases tension in the rat DA, the ability to sense a decrease in serum osmolality appears to be important for DA closure. We found that the hypoosmolality sensor TRPM3 was expressed in the DA tissues of humans and rats, and that TRPM3 is involved in hypoosmolality-induced DA contraction. TRPM3 is widely expressed in mammalian cells, including the collecting tubular epithelium of the kidney, pancreatic β-cells, neurons, and vascular SMCs.[31–34] Recently, Naylor *et al.*[32] reported the existence of a TRPM3 protein in the smooth muscle layer of the human saphenous vein and examined the functional role of TRPM3 in contractile responses in the mouse aorta. Majeed *et al.*[34] have also demonstrated TRPM3-mediated $[Ca^{2+}]_i$ increases in human vascular SMCs. These data are consistent with our finding that TRPM3 contributes to closure of the DA via increased $[Ca^{2+}]_i$. Although we have not examined whether a deficiency of TRPM3 would cause a failure of DA closure, the occurrence of PDA has not been reported in the studies on TRPM3 knockout mice.[35,36] In this context, the hypoosmolality-induced DA

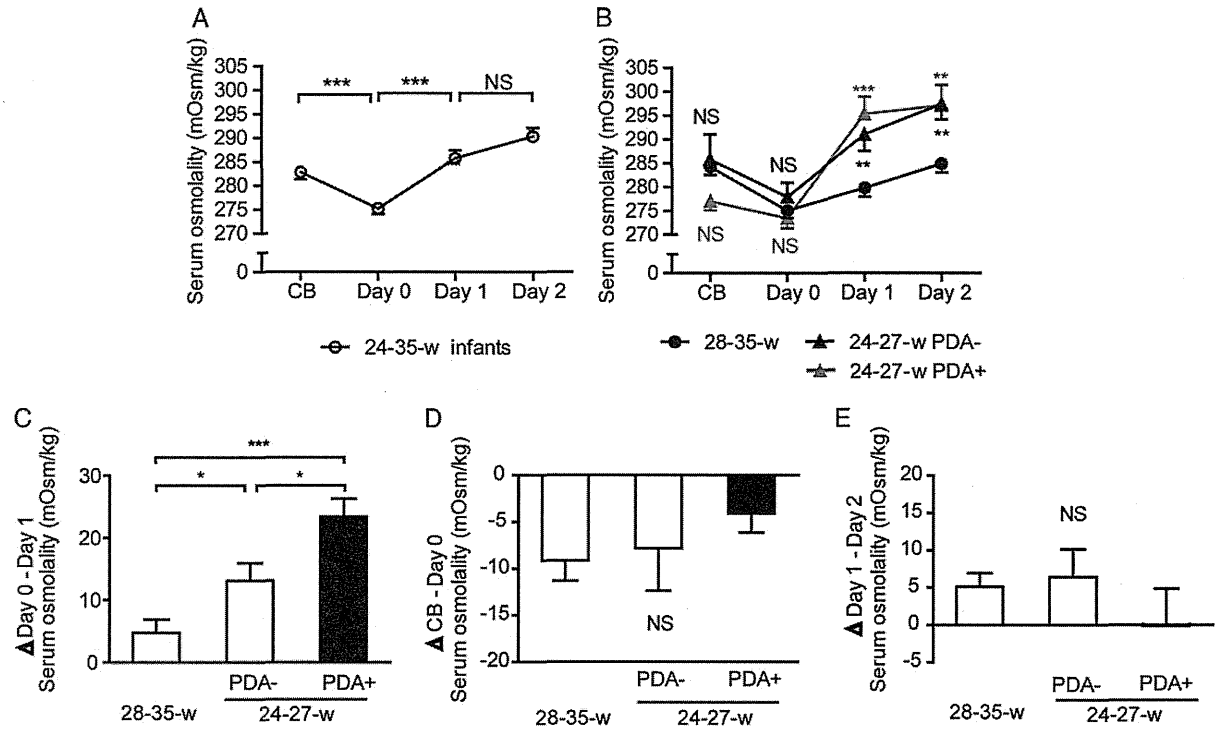

Figure 6 Changes in serum osmolality in human preterm infants. (*A*) Time course of serum osmolality in the entire preterm infant group born at 24- to 35-week gestation. $n = 62$, $^{***}P < 0.001$. NS: not significant. Osmolality was measured using a freezing-point depression osmometer. CB: cord blood. (*B*) Time courses of serum osmolalities in moderate- and late-preterm infants born at 28- to 35-week gestation ($n = 35$) and in extremely preterm infants born at 24- to 27-week gestation without PDA ($n = 12$) and with PDA ($n = 15$). $^{**}P < 0.01$; $^{***}P < 0.001$; NS: not significant vs. 28- to 35-week gestation. (*C*) Increase (Δ) in serum osmolality from Day 0 to Day 1 in extremely preterm infants with PDA born at 24- to 27-week gestation was larger than that in those without PDA at the same gestational age or moderate- and late-preterm infants born at 28- to 35-week gestation. $^{*}P < 0.05$; $^{***}P < 0.001$. (*D* and *E*) Changes from CB to Day 0 (*D*), and from Day 1 to Day 2 (*E*). NS: not significant.

closing mechanism, unlike the well-known oxygen-induced constriction mechanism, may not be the principal mechanism for DA closure. In addition to hypoosmolality-induced DA closure, our data suggested that *hyper*osmolality attenuates DA closure in a TRPM3-independent manner. Although previous reports demonstrated that hypertonic stimulation induced arterial dilatation via activation of potassium channels,[37,38] whether *hyper*osmolality-induced activation of potassium channels also promotes dilatation in the DA needs to be examined in the future.

Accumulating evidence suggests that TRPM3 could be regulated by pregnancy hormones and by the pharmacological treatment of PDA.[34,39] TRPM3 is known to be stimulated by physiological steroids including pregnenolone sulfate.[30] Majeed *et al.*[34] demonstrated that progesterone bonded to TRPM3 and inhibited endogenous TRPM3 activity in human vascular SMCs. It is of interest that foetuses are exposed to high levels of progesterone during the course of pregnancy, and that rapid withdrawal of this hormone occurs upon separation from the placenta.[40] Because our data demonstrated that TRPM3 mRNA was highly expressed in both premature and mature rat foetuses, it is tempting to speculate that TRPM3 might be kept inactive until birth by placental progesterone.

The mechanism by which serum osmolality is decreased at birth remains to be elucidated. However, two mechanisms, at least, may be considered. Serum osmolytes may be withdrawn through utilization and/or excretion via the kidneys at birth. Alternatively, osmolytes may be diluted in circulating blood. In this regard, we found that changes in serum osmolality were best correlated with those of Na^+ among other osmolytes, such as K^+, glucose, or BUN. Because serum Na^+ may not be utilized or excreted rapidly within an hour after birth, it is most likely that dilution of the circulating blood occurs. In the present study, there was no significant correlation between K^+, glucose, or BUN and osmotic changes. However, the data, which included a relatively small number of samples, did not negate the contributions of small amounts of K^+, glucose, and BUN to osmotic changes. This explanation agrees, at least in part, with previous studies demonstrating increased lung fluid clearance at respiratory onset: it has been shown that, immediately after birth, lung fluid shifts to the circulating blood compartment via aquaporins in the lung epithelium.[41,42] This may cause dilution of circulating blood, although lung fluid is also expelled mechanically at birth. The exact mechanisms of the transient decrease in serum osmolality, however, need to be further examined in future studies.

Our findings may also be of some practical use to paediatricians treating patients with PDA, i.e. serum osmolality should not be allowed to rise too high among extremely preterm infants with PDA. In general, such infants are likely exposed to increased serum osmolality. Because paediatricians are afraid of fluid overload and thus worsening of the patency of the DA simply due to circulating volume expansion,[43,44]

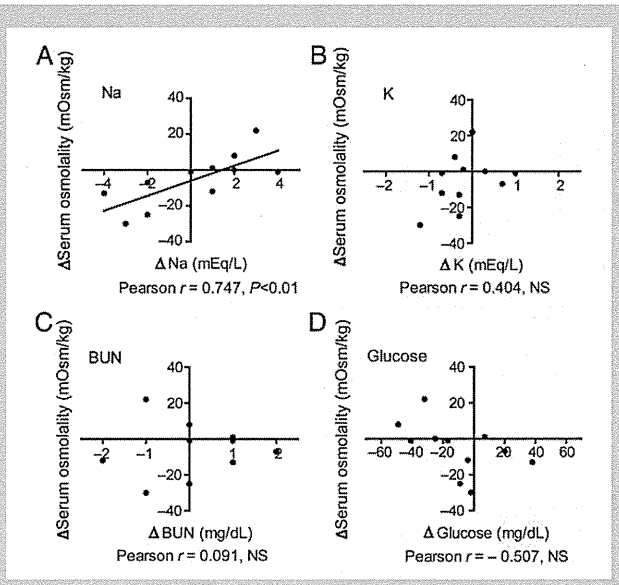

Figure 7 Relation between the degree of change in serum osmolality and that in osmolyte levels. (*A*) Degree of change in serum osmolality was correlated with that in Na^+ concentration in preterm infants ($n = 11$). *X*- and *Y*-axes indicate the degree of change in serum Na^+ concentration and that in serum osmolality, respectively, between Day 0 and Day 1–2. *r*: correlation coefficient. (*B–D*) Relation between the degree of change in serum osmolality and the degree of change in levels of three osmolytes in the same infants. *X*-axes in *B*, *C*, and *D* indicate the degree of changes in K^+, BUN, and glucose, respectively, and *Y*-axes indicate the degree of change in serum osmolality between Day 0 and Day 1–2. NS: not significant.

they tend to give fluid supplementation in smaller quantities. Furthermore, water evaporation and loss are greater among extremely preterm infants because of their immature and thin skin.[45] Concentrating urine is also insufficient, due to hypo-responsiveness to arginine vasopressin.[46] These factors may all contribute to increased serum osmolality among extremely preterm infants,[47] and thus might worsen PDA, as implied by our study. Thus, it seems reasonable to propose that keeping their serum osmolality at the proper, but not high, level may be important among preterm infants at risk for PDA.

In conclusion, serum osmolality is transiently decreased after birth, and this decrease may be a physiological mechanism to facilitate DA contraction. It may be time to reconsider the importance of serum osmolality in postnatal adaptation, especially among extremely preterm infants, who are most likely to develop PDA. Maintaining proper serum osmolality may be a clinically meaningful approach to improve the therapeutic outcome of such patients with PDA.

Supplementary material

Supplementary material is available at *Cardiovascular Research* online.

Acknowledgements

The authors are grateful to Yuka Sawada and Naoki Nicho for technical assistance.

Conflict of interest: none declared.

Funding

This work was supported by grants from The Japan Society for the Promotion of Science (grant nos: 22591205 to R.A.; 25293236, 24659100, and 23116514 to U.Y.; 25860614 to Y.Ic.; 23390277 to S.M.; 24390200, 25670131, and 22136009 to Y.Is.), and Shusanki-Iryoukankyou-Seibijigyou (support programmes to improve the Perinatal Care Environment Through Personnel Development) (R.A.), as well as by grants from the Ministry of Health, Labor and Welfare (Y.Is.), the Yokohama Foundation for Advanced Medical Science (U.Y., Y.Ic., and S.M.), the Takeda Science Foundation (U.Y., S.M., and Y.Is.), and a grant for the Research and Development Project of Yokohama City University (Y.Is.).

References

1. Noori S, Stavroudis T, Seri I. Principles of developmental cardiovascular physiology and pathophysiology. In: Kleinman CS, Seri I, eds. *Hemodynamics and Cardiology: Neonatology Questions and Controversies*. 2nd edn. Philadelphia: Elsevier Saunders; 2012. p. 3–27.
2. Koch J, Hensley G, Roy L, Brown S, Ramaciotti C, Rosenfeld CR. Prevalence of spontaneous closure of the ductus arteriosus in neonates at a birth weight of 1000 grams or less. *Pediatrics* 2006;**117**:1113–1121.
3. Nemerofsky SL, Parravicini E, Bateman D, Kleinman C, Polin RA, Lorenz JM. The ductus arteriosus rarely requires treatment in infants > 1000 grams. *Am J Perinatol* 2008;**25**: 661–666.
4. Hamrick SE, Hansmann G. Patent ductus arteriosus of the preterm infant. *Pediatrics* 2010; **125**:1020–1030.
5. Noori S, McCoy M, Friedlich P, Bright B, Gottipati V, Seri I, Sekar K. Failure of ductus arteriosus closure is associated with increased mortality in preterm infants. *Pediatrics* 2009;**123**:e138–e144.
6. Mirea L, Sankaran K, Seshia M, Ohlsson A, Allen AC, Aziz K, Lee SK, Shah PS. Treatment of patent ductus arteriosus and neonatal mortality/morbidities: adjustment for treatment selection bias. *J Pediatr* 2012;**161**:689–694.e1.
7. Clyman RI, Couto J, Murphy GM. Patent ductus arteriosus: are current neonatal treatment options better or worse than no treatment at all? *Semin Perinatol* 2012;**36**: 123–129.
8. Malviya MN, Ohlsson A, Shah SS. Surgical versus medical treatment with cyclooxygenase inhibitors for symptomatic patent ductus arteriosus in preterm infants. *Cochrane Database Syst Rev* 2013;**3**:CD003951.
9. Reeve HL, Tolarova S, Nelson DP, Archer S, Weir EK. Redox control of oxygen sensing in the rabbit ductus arteriosus. *J Physiol* 2001;**533**:253–261.
10. Michelakis E, Rebeyka I, Bateson J, Olley P, Puttagunta L, Archer S. Voltage-gated potassium channels in human ductus arteriosus. *Lancet* 2000;**356**:134–137.
11. Nakanishi T, Gu H, Hagiwara N, Momma K. Mechanisms of oxygen-induced contraction of ductus arteriosus isolated from the fetal rabbit. *Circ Res* 1993;**72**:1218–1228.
12. Yokoyama U, Minamisawa S, Adachi-Akahane S, Akaike T, Naguro I, Funakoshi K, Iwamoto M, Nakagome M, Uemura N, Hori H, Yokota S, Ishikawa Y. Multiple transcripts of Ca^{2+} channel alpha1-subunits and a novel spliced variant of the alpha1C-subunit in rat ductus arteriosus. *Am J Physiol Heart Circ Physiol* 2006;**290**:H1660–H1670.
13. Akaike T, Jin MH, Yokoyama U, Izumi-Nakaseko H, Jiao Q, Iwasaki S, Iwamoto M, Nishimaki S, Sato M, Yokota S, Kamiya Y, Adachi-Akahane S, Ishikawa Y, Minamisawa S. T-type Ca^{2+} channels promote oxygenation-induced closure of the rat ductus arteriosus not only by vasoconstriction but also by neointima formation. *J Biol Chem* 2009;**284**:24025–24034.
14. Smith GC. The pharmacology of the ductus arteriosus. *Pharmacol Rev* 1998;**50**:35–58.
15. Yokoyama U, Minamisawa S, Ishikawa Y. Regulation of vascular tone and remodeling of the ductus arteriosus. *J Smooth Muscle Res* 2010;**46**:77–87.
16. Yokoyama U, Iwatsubo K, Umemura M, Fujita T, Ishikawa Y. The prostanoid EP4 receptor and its signaling pathway. *Pharmacol Rev* 2013;**65**:1010–1052.
17. Jain L, Chen XJ, Ramosevac S, Brown LA, Eaton DC. Expression of highly selective sodium channels in alveolar type II cells is determined by culture conditions. *Am J Physiol Lung Cell Mol Physiol* 2001;**280**:L646–L658.
18. Bland RD. Loss of liquid from the lung lumen in labor: more than a simple 'squeeze'. *Am J Physiol Lung Cell Mol Physiol* 2001;**280**:L602–L605.
19. Modi N. Clinical implications of postnatal alterations in body water distribution. *Semin Neonatol* 2003;**8**:301–306.
20. Feldman W, Drummond KN. Serum and urine osmolality in normal full-term infants. *Can Med Assoc J* 1969;**101**:73–74.
21. Bourque CW, Oliet SH. Osmoreceptors in the central nervous system. *Annu Rev Physiol* 1997;**59**:601–619.
22. Liedtke W, Friedman JM. Abnormal osmotic regulation in $trpv4^{-/-}$ mice. *Proc Natl Acad Sci USA* 2003;**100**:13698–13703.
23. Grimm C, Kraft R, Sauerbruch S, Schultz G, Harteneck C. Molecular and functional characterization of the melastatin-related cation channel TRPM3. *J Biol Chem* 2003;**278**: 21493–21501.
24. Oberwinkler J, Phillipp SE. TRPM3. *Handbook Exp Pharmacol* 2007;**179**:253–267.

25. Yokoyama U, Minamisawa S, Quan H, Ghatak S, Akaike T, Segi-Nishida E, Iwasaki S, Iwamoto M, Misra S, Tamura K, Hori H, Yokota S, Toole BP, Sugimoto Y, Ishikawa Y. Chronic activation of the prostaglandin receptor EP4 promotes hyaluronan-mediated neointimal formation in the ductus arteriosus. *J Clin Invest* 2006;**116**:3026–3034.
26. Yokoyama U, Minamisawa S, Katayama A, Tang T, Suzuki S, Iwatsubo K, Iwasaki S, Kurotani R, Okumura S, Sato M, Yokota S, Hammond HK, Ishikawa Y. Differential regulation of vascular tone and remodeling via stimulation of type 2 and type 6 adenylyl cyclases in the ductus arteriosus. *Circ Res* 2010;**106**:1882–1892.
27. Straub I, Krugel U, Mohr F, Teichert J, Rizun O, Konrad M, Oberwinkler J, Schaefer M. Flavanones that selectively inhibit TRPM3 attenuate thermal nociception in vivo. *Mol Pharmacol* 2013;**84**:736–750.
28. Straub I, Mohr F, Stab J, Konrad M, Philipp SE, Oberwinkler J, Schaefer M. Citrus fruit and fabacea secondary metabolites potently and selectively block TRPM3. *Br J Pharmacol* 2013;**168**:1835–1850.
29. Hong Z, Hong F, Olschewski A, Cabrera JA, Varghese A, Nelson DP, Weir EK. Role of store-operated calcium channels and calcium sensitization in normoxic contraction of the ductus arteriosus. *Circulation* 2006;**114**:1372–1379.
30. Wagner TF, Loch S, Lambert S, Straub I, Mannebach S, Mathar I, Dufer M, Lis A, Flockerzi V, Philipp SE, Oberwinkler J. Transient receptor potential M3 channels are ionotropic steroid receptors in pancreatic beta cells. *Nat Cell Biol* 2008;**10**:1421–1430.
31. Lee N, Chen J, Sun L, Wu S, Gray KR, Rich A, Huang M, Lin JH, Feder JN, Janovitz EB, Levesque PC, Blanar MA. Expression and characterization of human transient receptor potential melastatin 3 (hTRPM3). *J Biol Chem* 2003;**278**:20890–20897.
32. Naylor J, Li J, Milligan CJ, Zeng F, Sukumar P, Hou B, Sedo A, Yuldasheva N, Majeed Y, Beri D, Jiang S, Seymour VA, McKeown L, Kumar B, Harteneck C, O'Regan D, Wheatcroft SB, Kearney MT, Jones C, Porter KE, Beech DJ. Pregnenolone sulphate- and cholesterol-regulated TRPM3 channels coupled to vascular smooth muscle secretion and contraction. *Circ Res* 2010;**106**:1507–1515.
33. Wagner TF, Drews A, Loch S, Mohr F, Philipp SE, Lambert S, Oberwinkler J. TRPM3 channels provide a regulated influx pathway for zinc in pancreatic beta cells. *Pflugers Arch* 2010; **460**:755–765.
34. Majeed Y, Tumova S, Green BL, Seymour VA, Woods DM, Agarwal AK, Naylor J, Jiang S, Picton HM, Porter KE, O'Regan DJ, Muraki K, Fishwick CW, Beech DJ. Pregnenolone sulphate-independent inhibition of TRPM3 channels by progesterone. *Cell Calcium* 2012;**51**:1–11.
35. Vriens J, Owsianik G, Hofmann T, Philipp SE, Stab J, Chen X, Benoit M, Xue F, Janssens A, Kerselaers S, Oberwinkler J, Vennekens R, Gudermann T, Nilius B, Voets T. TRPM3 is a nociceptor channel involved in the detection of noxious heat. *Neuron* 2011;**70**:482–494.
36. Hughes S, Pothecary CA, Jagannath A, Foster RG, Hankins MW, Peirson SN. Profound defects in pupillary responses to light in TRPM-channel null mice: a role for TRPM channels in non-image-forming photoreception. *Eur J Neurosci* 2012;**35**:34–43.
37. Ishizaka H, Kuo L. Endothelial ATP-sensitive potassium channels mediate coronary microvascular dilation to hyperosmolarity. *Am J Physiol* 1997;**273**:H104–H112.
38. Massett MP, Koller A, Kaley G. Hyperosmolality dilates rat skeletal muscle arterioles: role of endothelial K(ATP) channels and daily exercise. *J Appl Physiol* 2000; **89**:2227–2234.
39. Klose C, Straub I, Riehle M, Ranta F, Krautwurst D, Ullrich S, Meyerhof W, Harteneck C. Fenamates as TRP channel blockers: mefenamic acid selectively blocks TRPM3. *Br J Pharmacol* 2011;**162**:1757–1769.
40. Trotter A, Maier L, Pohlandt F. Management of the extremely preterm infant: is the replacement of estradiol and progesterone beneficial? *Pediatr Drugs* 2001;**3**:629–637.
41. Zelenina M, Zelenin S, Aperia A. Water channels (aquaporins) and their role for postnatal adaptation. *Pediatr Res* 2005;**57**:47R–53R.
42. Song Y, Ma T, Matthay MA, Verkman AS. Role of aquaporin-4 in airspace-to-capillary water permeability in intact mouse lung measured by a novel gravimetric method. *J Gen Physiol* 2000;**115**:17–27.
43. Stephens BE, Gargus RA, Walden RV, Mance M, Nye J, McKinley L, Tucker R, Vohr BR. Fluid regimens in the first week of life may increase risk of patent ductus arteriosus in extremely low birth weight infants. *J Perinatol* 2008;**28**:123–128.
44. Bell EF, Acarregui MJ. Restricted versus liberal water intake for preventing morbidity and mortality in preterm infants. *Cochrane Database Syst Rev* 2008;**1**:CD000503.
45. Hammarlund K, Sedin G, Stromberg B. Transepidermal water loss in newborn infants. VIII. Relation to gestational age and post-natal age in appropriate and small for gestational age infants. *Acta Paediatr Scand* 1983;**72**:721–728.
46. Bonilla-Felix M. Development of water transport in the collecting duct. *Am J Physiol Renal Physiol* 2004;**287**:F1093–F1101.
47. Baumgart S, Langman CB, Sosulski R, Fox WW, Polin RA. Fluid, electrolyte, and glucose maintenance in the very low birth weight infant. *Clin Pediatr (Phila)* 1982;**21**:199–206.

Med Mol Morphol
DOI 10.1007/s00795-014-0071-2

ORIGINAL PAPER

Establishment of successively transplantable rabbit VX2 cancer cells that express enhanced green fluorescent protein

Hisashi Oshiro · Hidenobu Fukumura · Kiyotaka Nagahama · Itaru Sato · Kei Sugiura · Hiroaki Iobe · Emi Okiyama · Toshitaka Nagao · Yoji Nagashima · Ichiro Aoki · Shoji Yamanaka · Ayumi Murakami · Jiro Maegawa · Takashi Chishima · Yasushi Ichikawa · Yoshihiro Ishikawa · Takeshi Nagai · Masaharu Nomura · Kenichi Ohashi · Koji Okudela

Received: 7 November 2013 / Accepted: 15 January 2014

Abstract Morphological detection of cancer cells in the rabbit VX2 allograft transplantation model is often difficult in a certain region such as serosal cavity where reactive mesothelial cells mimic cancer cells and both cells share common markers such as cytokeratins. Therefore, tagging VX2 cells with a specific and sensitive marker that easily distinguishes them from other cells would be advantageous. Thus, we tried to establish a successively transplantable, enhanced green fluorescent protein (EGFP)-expressing VX2 model. Cancer cells obtained from a conventional VX2-bearing rabbit were cultured in vitro and transfected with an EGFP-encoding vector, and then successively transplanted in Healthy Japanese White rabbits (HJWRs) ($n = 8$). Besides, conventional VX2 cells were transplanted in other HJWRs ($n = 8$). Clinicopathological comparison analyses were performed between the two groups. The success rate of transplantation was 100 % for both groups. The sensitivity and specificity of EGFP for immunohistochemical detection of VX2 cells were 84.3 and 100 %, respectively. No significant differences in cancer cell morphology, tumor size ($P = 0.742$), Ki-67 labeling index ($P = 0.878$), or survival rate ($P = 0.592$) were observed between the two. VX2 cells can be genetically altered, visualized by EGFP, and successively transplanted without significant alteration of morphological and biological properties compared to those of the conventional model.

Keywords Enhanced green fluorescent protein · Gene transfer technique · Rabbit · Shope papilloma virus · Carcinoma

Introduction

Supported by manageability and a broad understanding of genes, the use of mice or rats can substantially save space

H. Oshiro (✉) · K. Nagahama · Y. Nagashima · I. Aoki · S. Yamanaka · A. Murakami · K. Ohashi · K. Okudela
Department of Pathology, Yokohama City University Graduate School of Medicine, 3-9 Fukuura, Kanazawa-ku, Yokohama, Kanagawa 236-0004, Japan
e-mail: oshiroh@yokohama-cu.ac.jp

H. Oshiro · H. Iobe · E. Okiyama · T. Nagao · T. Nagai · M. Nomura
Department of Pathology, Tokyo Medical University Hospital, Tokyo, Japan

H. Fukumura
Department of Orthopaedic Surgery, Yokohama City University Graduate School of Medicine, Yokohama, Japan

I. Sato · K. Sugiura
Department of Oral and Maxillofacial Surgery, Yokohama City University Graduate School of Medicine, Yokohama, Japan

J. Maegawa
Department of Plastic and Reconstructive Surgery, Yokohama City University Graduate School of Medicine, Yokohama, Japan

T. Chishima · Y. Ichikawa
Department of Clinical Oncology and Breast Surgery, Yokohama City University Graduate School of Medicine, Yokohama, Japan

Y. Ishikawa
Department of Cardiovascular Research Institute, Yokohama City University Graduate School of Medicine, Yokohama, Japan

Published online: 27 February 2014

and time in animal experiments. While these rodents are invaluable for understanding the mechanisms of human diseases, other non-rodent models are required in certain situations. The rabbit is one such species that is widely used in biomedical research. The rabbit is more biologically similar to humans than rodents [1]. Additionally, because of the larger organs in rabbits, intricate surgical manipulation and imaging studies are easier to perform in rabbits than in mice or rats.

In oncology, the rabbit VX2 allograft cancer model is widely used not only in basic studies but also in preclinical and translational studies that cannot easily be performed in humans. The prototype for this model was derived from a virus-induced papilloma in rabbits [2], which subsequently progresses into a metastasizing carcinoma [3] that can be successively transplanted into other rabbits [4]. Subsequently, the loss of viral dependency of the tumors has been reported, and one of the tumors was denominated [5].

In this model, VX2 cancer cells proliferate in a host rabbit that maintains a natural immunity, which makes this model attractive and unique. Furthermore, this model replicates human peritoneal carcinomatosis well [6]. However, identification of the VX2 cancer cells is often difficult in regions such as serosal cavity or serosal membrane, where reactive mesothelial cells mimic VX2 cancer cells and both cells share common epithelial antigens such as cytokeratins. Therefore, tagging VX2 cancer cells with a simple, specific and sensitive marker that easily distinguishes them from other cells would be advantageous not only for accurate detection of the cells but also for saving time and cost in experiments.

Green fluorescent protein is a useful and reliable marker for visualizing live cells or molecules [7]. Theoretically, the green fluorescent protein gene transfer technique can be applied for the rabbit VX2 allograft cancer model, but no satisfactory model has been established to date. One reason for the absence of a model is likely that VX2 cancer cells are unstable ex vivo and easily lose transplantability after long-term cultivation or frozen storage [8–10]. Although some researchers have described a method for establishing a VX2 cell line [10–15], these cell lines are not routinely used for VX2 transplantation. This tendency is exemplified by the fact that a successive transplantation approach is still more common than the use of an experimental cell line [16]. This lack of available resources has prompted us to develop an appropriate and feasible methodology to insert an exogenous gene into VX2 cancer cells without using a VX2 cell line.

The aim of this study was to make a successively transplantable rabbit model of VX2 cancer cells that express enhanced green fluorescent protein (EGFP).

Materials and methods

Animals

A total of 22 Japanese white rabbits were used in this study. All animal procedures were performed in accordance with the approval and guidelines of the Institutional Animal Care and Use Committee of Yokohama City University (approval ID: F11-131, F-D-12-40). Each rabbit was individually housed, allowed free access to standard laboratory food and water, and maintained under a 12-h light/dark cycle per day at Yokohama City University Animal Center. During the experimental procedures, each rabbit was anesthetized by isoflurane inhalation using an anesthesia machine (SN-487-0T; Shinano Seisakujo; Tokyo, Japan). Euthanasia was administered to rabbits via cardiac injection of isoflurane after successive transplantation was performed.

As shown in Fig. 1, one VX2-bearing rabbit (Csk, Std; female; 15 weeks old; 3.2 kg; Japan SLC; Hamamatsu, Japan) was used as the original source of VX2 cells. Three healthy rabbits (Kbs; females; 8–14 weeks old; 2.0–2.8 kg; Oriental Yeast; Tokyo, Japan) were used as carriers for the preliminary transplantation. Two healthy rabbits (Kbs; females; 11 weeks old; 2.5 kg) were used for controls: one for the mock transfection control and the other for the cultured conventional VX2 transplantation control. Sixteen healthy rabbits (Kbs) were randomly allocated into two experimental groups for the comparison study: an EGFP gene-introduced VX2-transplanted rabbit group ($n = 8$) and a conventional VX2-transplanted rabbit group ($n = 8$). The EGFP gene-introduced VX2 group consisted of 6 females and 2 males, and the age was 12.8 ± 1.2 weeks (mean $\pm$ SE) and the weight was 2.51 ± 0.16 kg (mean $\pm$ SE) at the time of transplantation. The conventional VX2 group consisted of 6 females and 2 males, and the age was 14.9 ± 0.7 weeks (mean $\pm$ SE) and the weight was 2.86 ± 0.73 kg mean $\pm$ SE) at the time of transplantation. The rabbits in these two groups had no statistically significant differences in age ($P = 0.072$, unpaired Student's t test) or weight ($P = 0.156$, unpaired Student's t test). The primary end point for both experimental groups was defined as cancer growth, and the secondary end point was defined as death from cancer. Cancer growth was grossly inspected 3 weeks after transplantation, and the longest diameter of the tumor was measured with calipers. For the survival analysis, a total of 8 rabbits were reared without medical treatment from transplantation to death, and postmortem inspection was performed to determine the cause of death.

Plasmid preparation

Human embryonic kidney (HEK) 293T cells were grown in 100-mm culture dishes (Iwaki AGC Techno Glass; Funabashi, Japan) containing RPMI-1640 medium (Sigma-Aldrich Japan; Tokyo Japan) supplemented with heat-inactivated 10 % fetal bovine serum (FBS) (Sigma-Aldrich Japan), 100 units/ml of penicillin (Sigma-Aldrich Japan), and 0.1 mg/ml of streptomycin (Sigma-Aldrich Japan) in a 5 % CO_2 incubator at 37 °C.

EGFP complementary DNA was amplified by PCR with PrimeSTAR HS DNA polymerase (TakaraBio; Otsu, Japan) using the pIRES2-EGFP vector (Takara Bio) with the following mismatch primers containing EcoRI restriction sites: forward, 5′-ATGG*GAATTC*CCgggGTGAGCAAGGGCGAGGA-3′ (the first methionine [ATG] was converted to glycine [GGG], M1G) or 5′-ATGGaattcACCATGGTGAGCAAGGGCGAGGAG-3′; reverse, 5′-ATCTAG*GAATTC*GGCCGCTTTACTTGTA-3′ (the EcoRI restriction sites are italicized). The amplified EGFP cDNA was cut with EcoRI (TakaraBio) and inserted into the EcoRI site of the pQCXIP vector (TakaraBio). *E. Coli* DH5 competent cells (TakaraBio) were transformed with the EGFP gene-inserted pQCXIP vector and cultured according to the manufacturer's instructions.

The pQCXIP/EGFR vector and pCL10A1 retroviral packaging vector (TakaraBio) which expresses the 10A1 envelope protein under the control of the CMV immediate-early promoter were cotransfected into HEK 293T cells using the Lipofectamine 2000 reagent (Invitrogen, Carlsbad, CA, USA), according to the manufacturer's instructions. At 24 h after cotransfection, the conditioned medium was recovered from the dishes and used as a viral solution, as described below.

Primary culture of conventional VX2 cancer cells

After the fur was trimmed with an electric hair clipper and the skin surface was cleaned with rubbing alcohol, the conventional VX2 cancer tissue was cleanly excised from the thigh muscle of the rabbit with a sterile scalpel to avoid bacterial contamination from the environment. Trimming of the VX2 cancer tissue was performed with sterile scissors to eliminate other tissues and necrotic substances, and the tissue was washed twice in RPMI-1640 medium supplemented with an antibiotic and antimycotic mixed solution (Nacalai Tesque; Tokyo, Japan). The VX2 cancer tissue was then cut piece-by-piece in a sterile dish with sterile scissors. The cut surfaces of the VX2 cancer tissue were immediately imprinted onto sterile collagen type I-coated, 100-mm culture dishes (Iwaki AGC Techno Glass). The VX2 cancer cells were imprinted on a total of 30 culture dishes and were grown in 1 % FBS-containing RPMI-1640 medium with an antibiotic and antimycotic mixed solution in a 5 % CO_2 incubator at 37 °C.

Introduction of the EGFP gene into VX2 cancer cells and transplantation

On the fifth day after cultivation, the recovered viral solution was added to the VX2 culture dishes to introduce the EGFP gene into VX2 cancer cells, as shown in Fig. 1. At the same time, the VX2 culture medium was conditioned with 10 μg/ml of polybrene (Sigma-Aldrich Japan), and the VX2 culture dishes were incubated for 24 h for EGFP gene transduction. On the sixth day, the culture medium was replaced with 1 % FBS-containing RPMI-1640 containing antibiotics without polybrene, and the EGFP gene-introduced VX2 culture dishes were incubated for an additional 24 h. On the seventh day, the culture medium was replaced with 1 % FBS-containing RPMI-1640 with 10 μg/ml of puromycin (Invitrogen Japan; Tokyo, Japan), and the EGFP gene-introduced VX2 culture dishes were incubated for 2 days for the selection of EGFP gene-introduced VX2 cancer cells. On the ninth day, the rate of EGFP expression in VX2 cells was calculated by counting approximately 1,000 neoplastic cells in randomly selected high power fields under the fluorescence microscope. After removing all of the medium from the EGFP gene-introduced VX2 culture dishes, these dishes were washed twice with PBS (−) (Wako Pure Chemical; Osaka, Japan) and subjected to 0.25 % trypsin (Sigma-Aldrich Japan) treatment for 2 min in a CO_2 incubator at 37 °C. After adding 1 % FBS-containing RPMI-1640 to these dishes, the EGFP gene-introduced VX2 cancer cells were centrifuged at 800 rpm for 5 min, and the VX2 cells were resuspended with serum-free RPMI-1640 containing antibiotics, to a concentration of 1×10^6 VX2 cells/ml. 2 ml of the solution was inoculated into the thigh muscle of a healthy rabbit as a carrier. After 3 weeks, the EGFP gene-introduced VX2 cancer tissue was excised for further selection in puromycin, as described below.

Secondary culture of EGFP gene-introduced VX2 cancer cells for super-selection

For further selection, the EGFP gene-introduced VX2 cancer cells were cultured in 1 % FBS-containing RPMI-1640 medium with 10 μg/ml of puromycin. On the fourth day, the rate of EGFP expression in VX2 cells was calculated by counting approximately 1,000 neoplastic cells in randomly selected high power fields under the fluorescence microscope. After the super-selective, EGFP gene-introduced VX2 cancer cells were retrieved, 2×10^6 cells were injected into the thigh muscles of a healthy rabbit as a carrier.

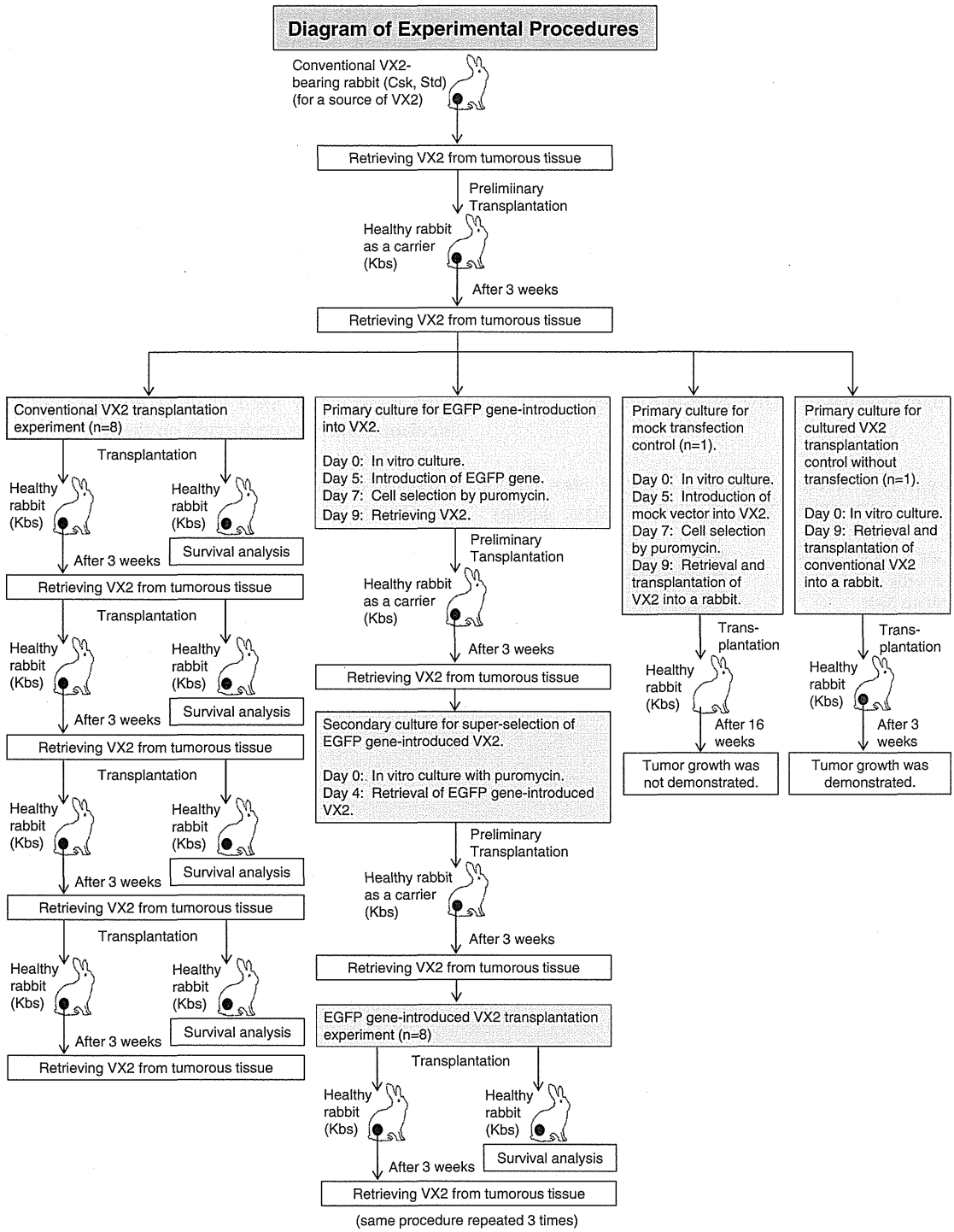

Fig. 1 Diagram of the experimental procedure for VX2 in vitro culture, EGFP gene-introduction, selection, and transplantation

Successive transplantation study of EGFP gene-introduced VX2 and conventional VX2

For the purpose of pathological study and survival analysis, successive transplantation of the super-selective, EGFP gene-introduced VX2 cells was carried out using the carrier rabbit as described above. Briefly, the tumor tissue was cleanly excised, trimmed, and cut into pieces. The VX2 cancer cells were collected through a sterile cell strainer (BD Falcon Cell Strainer 100 micron; Becton and